

ORIGINAL RESEARCH



A novel miR1983-TLR7-IFN β circuit licenses NK cells to kill glioma cells, and is under the control of galectin-1

Diana Shah ^{a,b,c,d*}, Andrea Comba ^{a,b,c,d*}, Syed M. Faisal ^{a,b,c,d*}, Padma Kadiyala ^{a,b,c,d}, Gregory J. Baker ^{a,b,c,d}, Mahmoud S. Alghamri ^{a,b,c,d}, Robert Doherty ^{a,b,c,d}, Daniel Zamler ^{a,b,c,d}, Gabriel Nuñez ^e, Maria G. Castro ^{a,b,c,d}, and Pedro R. Lowenstein ^{a,b,c,d}

^aDepartment of Neurosurgery, University of Michigan Medical School, Ann Arbor, MI, USA; ^bDepartment of Cell and Developmental Biology, University of Michigan Medical School, Ann Arbor, MI, USA; ^cRogel Cancer Center, University of Michigan, Ann Arbor, MI USA; ^dCancer Biology Training Program, University of Michigan Medical School, Ann Arbor, MI, USA; ^eDepartment of Pathology, University of Michigan Medical School, Ann Arbor, MI, USA

ABSTRACT

Although pharmacological stimulation of TLRs has anti-tumor effects, it has not been determined whether endogenous stimulation of TLRs can lead to tumor rejection. Herein, we demonstrate the existence of an innate anti-glioma NK-mediated circuit initiated by glioma-released miR-1983 within exosomes, and which is under the regulation of galectin-1 (Gal-1). We demonstrate that miR-1983 is an endogenous TLR7 ligand that activates TLR7 in pDCs and cDCs through a 5'-UGUUU-3' motif at its 3' end. TLR7 activation and downstream signaling through MyD88-IRF5/IRF7 stimulates secretion of IFN- β . IFN- β then stimulates NK cells resulting in the eradication of gliomas. We propose that successful immunotherapy for glioma could exploit this endogenous innate immune circuit to activate TLR7 signaling and stimulate powerful anti-glioma NK activity, at least 10–14 days before the activation of anti-tumor adaptive immunity.

ARTICLE HISTORY

Received 22 April 2021
Revised 31 May 2021
Accepted 31 May 2021

KEYWORDS

Glioblastoma; galectin-1; NK cells; TLR7; MyD88; IRF5; IRF7; IFN- β ; miR-1983

INTRODUCTION


Glioblastoma (GBM) is the most common and lethal primary brain malignancy with median survival below two years despite surgery, radiation, and chemotherapy.¹ Galectin-1 (Gal-1), a member of a family of β -galactoside-binding lectins, inhibits anti-tumor adaptive immunity by inducing apoptosis of cytotoxic T cells,^{2,3} and innate immunity of gliomas by facilitating NK cell evasion.^{4,5} The Cancer Genome Atlas (TCGA) and Chinese Glioma Genome Atlas (CGGA) datasets indicate that *LGALS1* (Gal-1) expression is significantly upregulated in GBM tumors and correlates with worst prognosis (Figure S1 (A-C)).

Understanding the mechanisms of immune suppression in gliomas is prerequisite to develop effective immunotherapies to improve outcomes for patients suffering from this devastating disease. Our previous studies in mice and rats gliomas uncovered a potent innate anti-glioma immune response mediated by NK cells and myeloid cells, which was inhibited by glioma-derived Gal-1.^{4,5} The mechanisms that sensitize Gal-1 deficient glioma cells (GL26-GAL1^{KD}) to NK killing remain unknown and are the subject of the current study.


We examined the growth of intracranial GL26-GAL1^{KD} gliomas in transgenic mice lacking specific components of

innate immunity. We discovered that TLR7-MyD88 signaling in myeloid derived pDCs and cDCs is necessary for NK mediated glioma rejection. Glioma rejection depended on IRF5, IRF7, IFN β , and IFNAR1 suggesting that IRF5 and IRF7 lead to IFN β release which, acting through IFNAR1 receptors licenses NK cells to kill glioma cells. These data strongly suggested the existence of a factor that was released from glioma cells and stimulated TLR7.

We thus searched for a putative endogenous ligand secreted by GL26-GAL1^{KD} cells and which could stimulate TLR7 signaling. We discovered that miR-1983 is released within exosomes by GL26-GAL1^{KD} glioma cells and is an endogenous ligand of TLR7 in myeloid cells. miR-1983 binds to TLR7 through a UGUUU motif to stimulate TLR7/MyD88 signaling via IRF5 and IRF7 resulting in IFN β release by dendritic cells which then stimulates NK cells through IFNAR1 to kill glioma cells. LDH5 plays a similar role in human NK cells, as it is secreted by glioma cells, and stimulates NK cytotoxicity.⁶ Our results demonstrate the existence of a putative miR1983-TLR7-IFN β -NK circuit in gliomas by which glioma cell themselves stimulate NK cells to kill the glioma cells, that is inhibited by Gal-1. We propose that stimulation of the miR1983-TLR7-NK circuit could be harnessed to recruit NK cells to kill gliomas.

CONTACT R. Lowenstein  pedrol@umich.edu  Department of Neurosurgery, University of Michigan Medical School, Ann Arbor, MI, USA; Department of Cell and Developmental Biology, University of Michigan Medical School, Ann Arbor, MI, USA; Rogel Cancer Center, University of Michigan, Ann Arbor, MI 48109, USA; Cancer Biology Training Program, University of Michigan Medical School, Ann Arbor, MI, USA

*These authors contributed equally to this work

 Supplemental data for this article can be accessed on the [publisher's website](#)

© 2021 The Author(s). Published with license by Taylor & Francis Group, LLC.

This is an Open Access article distributed under the terms of the Creative Commons Attribution-NonCommercial License (<http://creativecommons.org/licenses/by-nc/4.0/>), which permits unrestricted non-commercial use, distribution, and reproduction in any medium, provided the original work is properly cited.

RESULTS

NK cells eradicate Gal-1 deficient (GL26-GAL1^{KD}) glioma

We have previously demonstrated that rejection of intracranial GL26-GAL1^{KD} tumors depends on NK cells.⁴ To do so we demonstrated that immunodepletion of NK cells by anti-NK1.1 and anti-ASGM1 antibodies in Rag1^{-/-} (which lacks T and B cells but not NK cells) abrogated the elimination of GL26-GAL1^{KD} tumor. However, to validate the absolute involvement of NK cells in the glioma rejection, this time we used the more stringent transgenic model Rag2/IL2rg which lacks B cells, T cells as well as functional NK cells. The general experimental design is depicted in Figure 1a. We quantified GL26-GAL1^{KD} glioma growth in Rag2/IL2rg knockout mice. Our data showed significant tumor growth in Rag2/IL2rg knockout mice compared to control mice (C57BL6/J) (Figure 1b) and Rag2 mice which lack T and B cells but not NK cells (Figure S2C). Concomitantly, we have previously demonstrated that depletion of NK cells in fully immunocompetent C57BL/6 mice by repeated administration of either anti-NK1.1 antibodies or ASGM1 (anti-Asialo GM1) serum, allows GL26-GAL1^{KD} glioma growth (Figure 1b) as previously shown in⁴ served as a control for NK immunodepletion. Altogether, these results identify NK cells as effector cells in the rejection of GAL1^{KD} gliomas by the innate immune system.

IFN-β through IFNAR1 receptor induces GL26-GAL1^{KD} glioma rejection

Next, we addressed the question of potential effector mechanisms responsible for NK-mediated glioma rejection. The interaction of the activating NK cell receptor NKG2D with NKG2D ligands which are expressed in stressed or transformed cells, has been shown to be a very important mechanism of NK cell recognition and rejection of tumor cells in general.^{7,8} Therefore, we tested whether GL26-GAL1^{KD} gliomas would be rejected in NKG2D^{-/-} mice. However, lack of the activating NK cell receptor NKG2D has a very minor role, even if statistically significant in the rejection of gliomas (Figure 1b), indicating that rejection of GL26-GAL1^{KD} gliomas is mostly not dependent on NKG2D. Nevertheless, NK-mediated killing involves various activating receptors including Nkp46, Nkp30, Nkp44, DNAM-1 and NKG2D.^{9,10} The role of NK activating receptors, beyond NKG2D, will be explored in future experiments. In the Perforin^{-/-} mice GL26-GAL1^{KD} gliomas showed significant increased glioma growth compared to control animals (Figure 1b) indicating that glioma rejection is mediated in part by perforin released from cytolytic NK cell granules.

We then analyzed the growth of GL26-GAL1^{KD} gliomas in transgenic mice which lacked either IFNγ or the receptor for IFNγ (IFNγR1). Although, IFNγ is known to be one of the effector molecules secreted subsequently to NK cell activation,^{11,12} it had a small and statistically significant effect on growth of GL26-GAL1^{KD} gliomas (Figure 1b). The difference in tumor growth in IFNγR1 deficient mice compared to control mice was not statistically significant. This indicates that

in our tumor model, recognition and rejection of GL26-GAL1^{KD} tumors is partially dependent on perforin and IFNγ.

To further identify which effector molecules are engaged in the rejection of GL26-GAL1^{KD} gliomas, we analyzed growth of GL26-GAL1^{KD} gliomas in transgenic mice lacking TNFRI/II (Figure 1b). Although, growth of GL26-GAL1^{KD} gliomas in the absence of TNFRI/II was significant, but the effect was much smaller compared to perforin^{-/-} and IFNγ^{-/-} groups (Figure 1b), suggesting a very minor role in the rejection of GL26-GAL1^{KD} tumors.

To determine which receptors are involved in the rejection of GL26-GAL1^{KD} gliomas, we analyzed growth of GL26-GAL1^{KD} gliomas in murine models treated with antibodies to block IFNAR (Figure 1b). The data showed that abrogation of type I interferon signaling had a strong effect and resulted in significant growth of GL26-GAL1^{KD} gliomas (Figure 1b). To address the question of which type I interferon is involved, we further assessed whether the rejection is IFN-α or IFN-β mediated. We monitored the growth of GL26-GAL1^{KD} gliomas in the experimental murine model depleted of either IFN-α or IFN-β, and depleted of both IFN-α + IFN-β, employing appropriate monoclonal antibodies. Our data demonstrate that significant tumor growth was observed in the IFN-β depleted murine model compared to IFN-α depleted mice (Figure 1c), and the IFNα+IFN-β combined depletion (Figure 1c). We illustrate GL26-GAL1^{KD} glioma growth which expanded into the whole striatum in IFN-β deficient mice, compared to IFN-α deficient mice, emphasizing the significance of IFN-β for glioma rejection (Figure 1d). This establishes that IFN-β is the key type I interferon which mediates the rejection of GL26-GAL1^{KD} gliomas.

GL26-GAL1^{KD} glioma rejection is independent of the cGAS-STING pathway

We next tested the effect of other cytokines involved in anti-tumor immune response, i.e. the interleukin IL-12, IL-1 and IL-18 signaling on GL26-GAL1^{KD} gliomas growth. There were no differences observed in tumor growth in the absence or presence of IL-1 R or IL-18 (Figure S2A), however, growth of GL26-GAL1^{KD} gliomas in the absence of IL-12 (Figure S2A) was significant but the effect was very small thus unlikely to be of biological significance.

Additionally, we further tested the growth of GL26-GAL1^{KD} gliomas in the absence of MHCI, CCL2, CCR5, CXCR3, CCR2, CX3CR1, mast cell, γδ T cells, and cGAS-STING pathway components. There were no significant differences observed in glioma growth in the absence of CCR5, CXCR3, CCR2, CX3CR1, mast cell, γδ T cells, and cGAS-STING pathway (Figure S2B). However, glioma growth was increased in the absence of MHCI and CCL2 but the effect was modest (Figure S2B). This shows that MHCI and CCL2 has a minor role in recognition and rejection of GL26-GAL1^{KD} gliomas in our tumor model. A summary of the comprehensive screening of GL26-GAL1^{KD} glioma growth in transgenic mice lacking specific

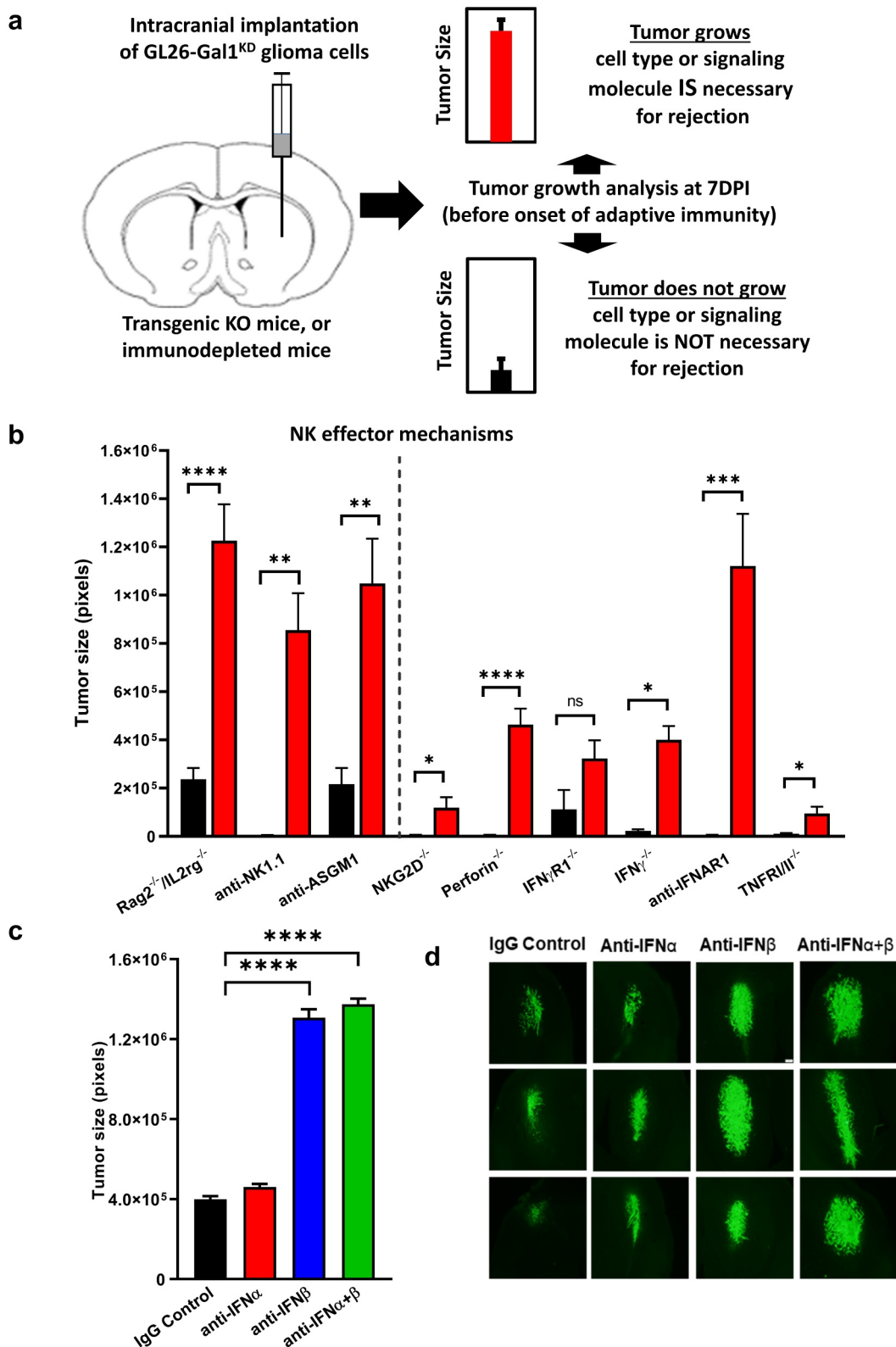


Figure 1. Gal-1 deficient glioma is rejected by NK cells through IFN-β/IFNAR1 signaling. (a) Illustration of experimental design to analyze galectin-1 deficient (GL26-GAL1^{KD}) glioma growth in transgenic knockout or immunodepleted mice. (b) Quantification of tumor size (in pixels) in Rag2^{-/-}/IL2rg^{-/-} mice (which lack B cells, T cells, as well as functional NK cells), NK-immunodepleted mice with anti-NK1.1 or anti-ASGM1, or mice lacking the specific molecule of NK effector signaling pathway (i.e., NKG2D^{-/-}, perforin^{-/-}, IFNγR1^{-/-}, IFNγ^{-/-}, TNFR1/II^{-/-}), and IFNAR1 immunodepleted mice after 7DPI. Control mice (C57BL/6 J) are shown in black while transgenic and immunodepleted mice are shown in red. Data are shown as mean ± SEM. *p < .05, **p < .01, ***p < .001, and ****p < .0001 versus respective control groups (one-way ANOVA). (c) Quantification of tumor size (in pixels) in immunodepleted mice for IFN-α or IFN-β or both IFN-α + IFN-β compared to IgG isotype treated control group. Data are represented as mean ± SEM. *p < .05, **p < .01, ***p < .001, and ****p < .0001 versus respective control group (one-way ANOVA). (d) Representative fluorescence micrograph of GL26-GAL1^{KD} glioma growth implanted in immunodepleted mice for IFN-α or IFN-β or both IFN-α + IFN-β.

molecules of immune signaling, in the form of a master graph is shown in Figure S2C.

GL26-GAL1^{KD} glioma derived conditioned medium activates NK cells

To identify the source of NK cell stimulation derived from GL26-GAL1^{KD} cells, we investigated the effect of conditioned medium from GL26-GAL1^{KD} gliomas (CM-GAL1^{KD}) on the activation of NK cells using wildtype (wt) splenocytes. This resulted in a strong and statistically significant increase of the expression of the activation marker CD69 on NK cells when compared with conditioned medium from Gal-1 expressing GL26-GAL1^{WT} glioma (CM-GAL1^{WT}) (Figure S2D). Our flow cytometry gating strategy is shown in Figure S3A.

TLR7 signaling is necessary for NK cell mediated rejection of GL26-GAL1^{KD} glioma

Toll-like receptor (TLR) signaling is one of the major pathways involved in activation of the innate immune system.^{13–16} We investigated the role of TLRs in the rejection of GL26-GAL1^{KD} glioma in transgenic mice lacking MyD88 or TRIF. MyD88 is a key adaptor molecule in the activation of downstream signaling of TLRs 1, 2, 4, 5, 6, 7, 8, and 9 whereas TRIF is involved in downstream signaling of TLR4 and TLR3.^{16–20} Rejection of intracranial GL26-GAL1^{KD} gliomas was abrogated in the absence of MyD88 but not in TRIF^{-/-} mice (Figure 2a), indicating that signaling through a MyD88-dependent TLR is required for rejection. To identify the exact TLR involved, we implanted GL26-GAL1^{KD} gliomas into transgenic mice lacking one particular (TLR7, TLR5 or TLR9) or a combination of two different (TLR2 and TLR4) MyD88-dependent TLRs. Analysis of 7 dpi GL26-GAL1^{KD} glioma growth in transgenic mice that lack TLR5, TLR9, or TLR2/4 did not affect rejection of GL26-GAL1^{KD} gliomas (Figure 2a). In contrast, mice lacking TLR7 exhibited enhanced tumor growth (Figure 2a). This suggests that TLR7 signaling is essential for the rejection of GL26-GAL1^{KD} gliomas. As illustrated in Figure 2b GL26-GAL1^{KD} tumors expanded into the whole striatum in TLR7 knockout mice, compared to wt mice (C57BL/6), emphasizing the significance of TLR7 for GL26-GAL1^{KD} glioma rejection.

To further determine downstream signaling molecules involved in TLR7-mediated GL26-GAL1^{KD} glioma rejection, we analyzed GL26-GAL1^{KD} gliomas growth in Interferon-related factors (IRF5^{-/-} and IRF7^{-/-}) mice. IRF 5 and IRF7 are important transcription factors downstream of TLR7. In the absence of IRF7, mice showed an increase in tumor growth compared to wt controls, but overall the effect was very small, indicating that IRF7 signaling only plays a minor role (Figure 2a). In contrast, rejection of GL26-GAL1^{KD} tumors was abolished in IRF5^{-/-} mice, resulting in large intracranial tumors compared to respective control group (Figure 2a). This indicates that the activating signaling downstream of TLR7 and its adaptor molecule MyD88 is mediated mainly by IRF5 with a minor contribution of IRF7.

To test whether CM-GAL1^{KD} induces direct NK cell activation in a TLR7 dependent manner, we measured CD69 expression on NK cells in wt vs TLR7^{-/-} splenocytes in response to

CM-GAL1^{KD}. We also included control groups treated with TLR7-specific (R848, Imiquimod, Loxoribine) or TLR3-specific (poly I:C) synthetic agonists. Our data showed that TLR7 agonists R848, Loxoribine, or Imiquimod significantly increased CD69 expression on NK cells in wt splenocytes compared to controls. To demonstrate the functionality of NK cells from both wt and TLR7^{-/-} splenocytes preparations, we treated them with TLR3-specific poly I:C agonist which induce comparable CD69 expression on NK cells (Figure 2c). CD69 expression on NK cells in wt splenocytes is comparable to the TLR7^{-/-} splenocytes in the unstimulated control group. The lack of CD69 induction on NK cells in CM-GAL1^{WT} treated groups confirmed that the ligand for TLR7 is present only in the CM-GAL1^{KD}. Importantly, lack of CD69 expression on NK cells in TLR7^{-/-} splenocytes in response to co-culture with CM-GAL1^{KD} demonstrates TLR7 specificity of conditioned medium derived from GL26-GAL1^{KD} glioma cells.

Next, we analyzed TLR7 expression on NK cells and different myeloid cell populations present in splenocytes using flow cytometry to determine the differential expression of TLR7 across splenocytes populations. We found that 100% of pDCs (CD45⁺CD11c⁺PDCA1⁺B220⁺), 77% of cDCs (CD45⁺CD11c⁺PDCA1⁻B220⁻), 63.7% of macrophages (CD11b⁺F4/80⁺), and 67.7% of monocytic Gr-1^{low}CD11b⁺ expressing myeloid cells express TLR7 in contrast to only 7.26% of the Gr-1^{high}CD11b⁺ myeloid cells and 7.53% of NK cells (Figure 2d). Moreover, to demonstrate specificity of the TLR7 staining, we also included the TLR7^{-/-} splenocytes as a negative control (middle panel of Figure 2d). The very low expression of TLR7 on NK cells precludes a direct effect of CM-GAL1^{KD} on NK cells, and strongly supports the need for an accessory cell to induce anti-glioma NK cytotoxicity.

pDCs and cDCs are necessary to reject GL26-GAL1^{KD} gliomas: *in vitro* and *in vivo* studies

We have previously demonstrated strong recruitment of bone marrow-derived tumor infiltrating myeloid DCs (mDCs) and pDCs to the Tumor immune microenvironment of GL26 gliomas in response to immune-stimulatory gene therapy (Ad-TK + Ad-Flt3L).^{21,22} Additionally, we have recently demonstrated that immunodepletion of Gr-1⁺ myeloid cells in RAG1^{-/-} permits the growth of GAL1^{KD} glioma despite the presence of NK cells, thus demonstrating an essential role for myeloid cells in the rejection of GL26-GAL1^{KD} gliomas.⁵ To determine which accessory cells are involved in the NK rejection, we assessed the expression of activation marker CD69 on CD45⁺CD3⁻NK1.1⁺ NK cells within the whole population of splenocytes (including all the immune cells) and within magnetically activated cell sorting (MACS)-enriched NK cells treated with CM-GAL1^{KD}. MACS resulted in an enriched population of NK cells (91.5% purity) vs 2.3% prior to enrichment (Figure 3a). Incubation of whole splenocytes with CM-GAL1^{KD} resulted in increased CD69 expression on NK cells when compared with unstimulated cells (Figure 3b). In contrast, isolated enriched NK cells were not stimulated by CM-GAL1^{KD} (Figure 3b). We also included a positive control in which we stimulated the enriched NK cells with a combination of IL-12+ IL-15 which resulted in

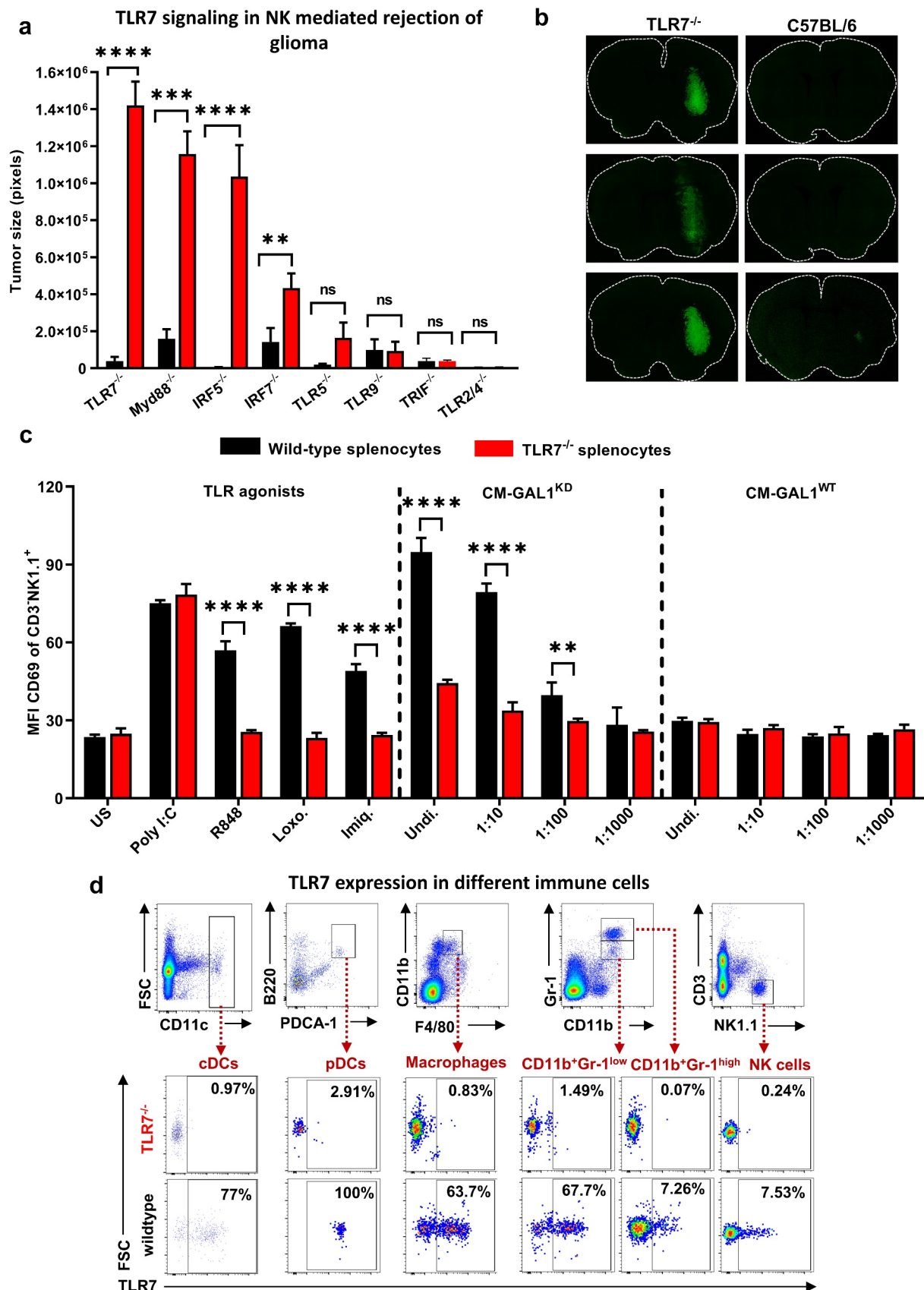


Figure 2. NK cells eradicate GL26-GAL1^{KD} glioma through TLR7 signaling. (a) Quantification of GL26-GAL1^{KD} glioma tumor size (in pixels) in transgenic mice lacking one particular (TLR7, TLR5 or TLR9) or a combination of two different (TLR2 and TLR4) MyD88-dependent TLRs or IRF5^{-/-} or IRF7^{-/-} or in TRIF^{-/-} mice in red and respective wt controls (C57BL/6 J) are shown in black. Data are represented as mean ± SEM. *p < .05, **p < .01, ***p < .001, and ****p < .0001 versus respective control group (one-way ANOVA) after 7DPI. (b) Representative fluorescence micrographs of GL26-GAL1^{KD} glioma growth in the striatum of TLR7^{-/-} mice vs C57BL/6 J as a wt control after 7DPI. Glioma growth is seen in each TLR7^{-/-} transgenic mouse (green fluorescent), conversely, only a scar at the initial tumor implantation site is observed in C57BL/6 J. (c) Flow cytometric analysis of CD69 expression on CD3-NK1.1⁺ NK cells after co-culture of splenocytes from (C57BL/6 J) wt or TLR7^{-/-} mice with CM-

GAL1^{KD} or CM-GAL1^{WT}. Control groups are either stimulated with TLR7 agonists (R848, Loxoribine, or Imiquimod) which served as a positive control or with fresh media (unstimulated controls). To demonstrate functionality of NK cells from both splenocytes preparations, we included a control group that was stimulated with a TLR3 agonist (poly I:C). NK cells of wt as well as TLR7^{-/-} mice responded with increased CD69 expression to TLR3-specific stimulation, compared to US. Middle panel shows the co-culture of splenocytes with a serial dilution of CM-GAL1^{KD} with fresh medium at 1:10, or 1:100, or 1:1000. Right panel shows the co-culture of splenocytes with a serial dilution of CM-GAL1^{WT} with fresh medium at 1:10, or 1:100, or 1:1000. Wt splenocytes are shown in black while TLR7^{-/-} are shown in red. CD69 expression is shown as mean fluorescent intensity (MFI) in the bar graph. Data are represented as mean \pm SEM. **p* < .05, ***p* < .01, ****p* < .001, and *****p* < .0001 versus respective control group (one-way ANOVA). (d) Representative flow cytometric plots of TLR7 expression on CD3⁻NK1.1⁺ NK cells, or CD45⁺CD11c⁺PDCA1⁺B220⁻ pDCs, or CD45⁺CD11c⁺PDCA1⁻B220⁻ cDCs or in monocytic Gr-1^{low}CD11b⁺ expressing myeloid cells, or CD11b⁺F4/80⁺ macrophages or Gr-1^{high}CD11b⁺ cells from wt C57BL/6 J controls vs TLR7^{-/-} splenocytes.

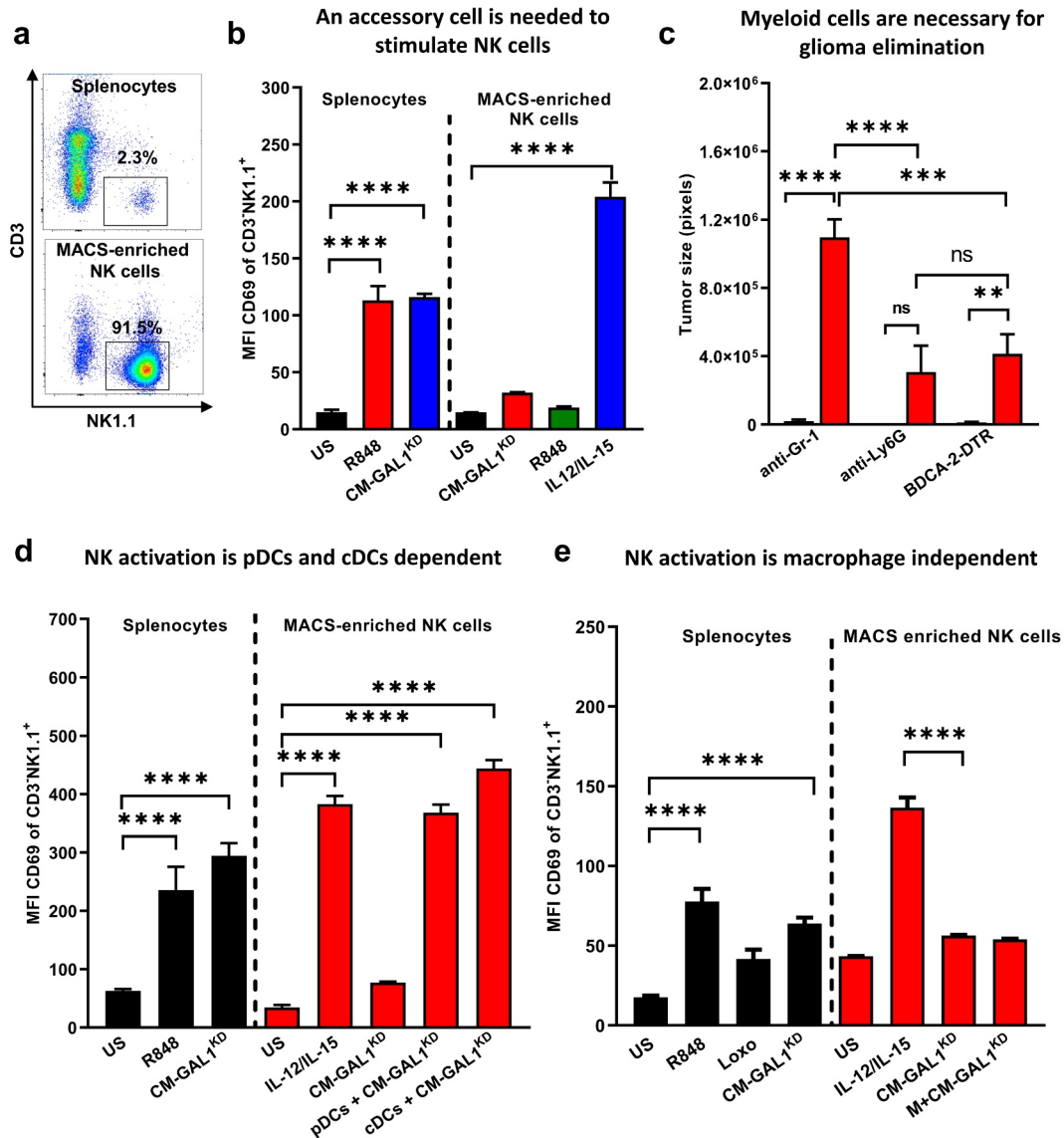


Figure 3. pDCs and cDCs are essential for the activation of NK cells. (a) Representative flow cytometry plots of CD3⁻NK1.1⁺ NK cells population in splenocytes vs magnetically activated cell sorting (MACS) enriched NK cells. (b) Flow cytometric analysis of CD69 expression on CD3⁻NK1.1⁺ NK cells within whole splenocytes preparations or on MACS enriched NK cells. Whole splenocytes or MACS enriched NK cells was incubated with CM-GAL1^{KD} or R848, a TLR7 agonist. (R848) served as a positive control for whole splenocytes while fresh medium treated served as unstimulated controls (US). IL12/IL15 treatment served as a positive control for NK cells alone (MACS enriched). CD69 expression is shown as mean fluorescent intensity (MFI) in the bar graph. Data are represented as mean \pm SEM. **p* < .05, ***p* < .01, ****p* < .001, and *****p* < .0001 versus respective control group (one-way ANOVA). (c) Quantification of GL26-GAL1^{KD} glioma tumor size (in pixels) in immunodepleted Gr-1 expressing myeloid cells by repeated administration of an anti-Gr-1 antibody mice or immunodepleted Ly6G-expressing myeloid or in BDCA-2-DTR transgenic mice. Depletion of plasmacytoid dendritic cells (pDCs) in BDCA-2-DTR mice was performed by intraperitoneal injections of 100 ng diphtheria toxin on days -1, 1, 3, 5 DPI. Wt C57BL/6 J controls are shown in black while immunodepleted or transgenic mice are shown in red. (d-e) To identify the essential accessory cells, we co-cultured MACS-enriched NK cells with pDCs or cDCs (d) or macrophages (e) in the presence of CM-GAL1^{KD}. R848, a TLR7 agonist. (R848) served as a positive control for whole splenocytes while fresh medium treated served as unstimulated controls (US). IL12/IL15 treatment served as a positive control for NK cells alone (MACS enriched). CD69 expression is shown as mean fluorescent intensity (MFI). Data are represented as mean \pm SEM. **p* < .05, ***p* < .01, ****p* < .001, and *****p* < .0001 versus respective control group (one-way ANOVA).

an increase of CD69 expression (Figure 3b). These results extend our previous findings showing that the NK cell

activation by CM-GAL1^{KD} is indirect, and dependent on an accessory cell.⁵

We have previously shown that depletion of Gr-1 expressing myeloid cells by administration of an anti-Gr-1 antibody abolished tumor rejection and resulted in significant tumor growth.⁵ In contrast, depletion of Ly6G-expressing myeloid cells did not show a significant effect on tumor growth (Figure 3c), indicating that the effect seen after Gr-1 depletion might be mainly mediated by monocytic Ly6C (Gr-1^{low}) expressing myeloid cells.

To characterize the accessory cells involved we further tested the role of plasmacytoid dendritic cells (pDCs) in the rejection of GL26-GAL1^{KD} gliomas using a transgenic murine model in which diphtheria toxin receptor (DTR) is expressed under a pDCs-specific promoter (BDCA-2-DTR mice). Administration of diphtheria toxin results in depletion of pDCs. The effect of pDC depletion on GL26-GAL1^{KD} gliomas growth was significant but smaller compared to the anti-Gr-1 depleted group (Figure 3c), suggesting that GL26-GAL1^{KD} glioma rejection is mediated in part by pDCs.

To characterize the direct involvement of accessory cells in NK cell activation *in vitro*, we sorted pDCs (CD45⁺CD11c⁺PDCA1⁺B220⁺), cDCs (CD45⁺CD11c⁺PDCA1⁻B220⁻) and macrophages (CD11b⁺F4/80⁺) from splenocytes, using flow cytometry. We co-cultured the MACS-enriched NK cells with pDCs, cDCs, or macrophages treated with CM-GAL1^{KD}. Co-culturing of pDCs as well as cDCs with MACS-enriched NK cells showed large increases of CD69 expression on NK cells respectively, in the presence of CM-GAL1^{KD} (Figure 3d), while basal level was observed in the macrophage co-cultured group (Figure 3e), indicating macrophages are not involved in the glioma rejection. These results suggest that pDCs and cDCs are accessory cell subsets required for NK cell activation within the innate anti-glioma immune circuit stimulated by CM-GAL1^{KD}.

Glioma cells release exosomes containing an endogenous TLR7 ligand

Our data show that NK cell activation by conditioned medium derived from GL26-GAL1^{KD} glioma is dependent on TLR7 present in an accessory cell. TLR7 is an endosomal sensor that recognizes ssRNA molecules.²³ To determine whether GL26-GAL1^{KD} glioma release an endogenous RNA TLR7 ligand, we co-cultured splenocytes with activating CM-GAL1^{KD} pre-treated with RNase A (5 U/ml) for 30 min at 37°C and assessed CD69 expression on NK cells (Figure 4a). RNase treatment did not affect the activating capacity of CM-GAL1^{KD}, suggesting that an endogenous RNA TLR7 ligand is not present as free single-stranded RNA in the conditioned medium. Alternatively, a RNA TLR7 ligand could be protected from RNase if located within vesicles such as exosomes.

To examine this hypothesis, we established a protocol to separate exosomes from the conditioned medium using ultracentrifugation (Figure 4b). Separate preparations of exosomes, and exosome-depleted supernatant were tested for their capacity to induce NK activation (Figure 4c). We also included an unstimulated control (US), and R848, a TLR7 agonist as a positive control. Co-incubation with R848 or CM-GAL1^{KD} resulted in enhanced CD69 expression on NK cells compared to unstimulated controls. Interestingly, GL26-GAL1^{KD} gliomas

derived exosomes significantly induced CD69 expression on NK cells compared to exosome-free conditioned medium (Figure 4c). In comparison, CM-GAL1^{WT} or GL26-GAL1^{WT} glioma derived exosomes, or exosome-free conditioned supernatant were not able to induce CD69 expression on NK cells (Figure 4c).

To identify the TLR7 ligand, exosomes were precipitated from the conditioned medium from GL26-GAL1^{KD} or GL26-GAL1^{WT} glioma. miRNA was then isolated from the respective exosomes and sequenced. We identified a set of 14 differentially expressed miRNAs as shown in the Volcano Plot in Figure 4d, and in a Heatmap in Figure 4e. The Volcano plot shows the levels of expression and the significance of such changes. The Heatmap illustrates that miRNAs fall into two categories depending on their origin. Ten miRNAs were upregulated (red) and four were downregulated (green). The most highly differentially expressed miRNAs are highlighted in red (described in detail in Table S1).

Taken together our experiments strongly suggest that short RNAs such as miRNAs within exosomes released from GL26-GAL1^{KD} glioma cells are potentially responsible for stimulating TLR7 present in the myeloid cells to initiate an innate anti-glioma NK mediated immune response.

GL26-GAL1^{KD} glioma derived exosomal miR-1983 triggers TLR7 mediated NK activation

We utilized miRNA sequencing data to select and test candidate miRNAs to discover a potential ligand responsible for the TLR7 mediated NK activation. We measured expression of the activation marker CD69 on CD45⁺CD3⁻NK1.1⁺ gated NK cells in response to synthetic miRNAs agonists (Figure 5a). Our data revealed that miR-1983 had the strongest activating effect, followed by miR-183-5p and miR-181b-5p (Figure 5a), and miR-1983 was therefore later chosen for further molecular studies of binding to TLR7.

To determine whether NK cell activation in response to miRNAs treatment is TLR7 specific, we incubated the differentially upregulated miRNAs synthetic agonists and other control TLR7 agonists with splenocytes isolated from the C57BL/6 (wt) or TLR7^{-/-} mice. Only C57BL/6 splenocytes exhibited CD69 induction on CD45⁺CD3⁻NK1.1⁺ gated NK cells in response to miRNAs agonists miR-1983, miR-183-5p, miR-181b-5p, while TLR7^{-/-} splenocytes (TLR7KO) didn't respond to the miRNA agonists or to the positive control R848 (Figure 5b).

miR-1983 stimulated NK cells mediate glioma killing

To assess the functional cytotoxicity of activated NK cells we stimulated splenocytes with miR-1983 and after 18 h of , we enriched NK cells employing MACS. MACS achieved an NK cells enrichment from 1.25% to 78.3% in unstimulated, 73.4% in R848 stimulated and 69.8% in miR-1983 treated group (Figure 5c). We co-cultured the treated MACS-enriched NK cells from various groups with GL26-GAL1^{KD} glioma cells. Our data showed 94% of the GL26-GAL1^{KD} glioma cells undergo lysis in response to miR-1983 pre-activated NK cells. Furthermore, 71% of the GL26-GAL1^{KD} glioma cells undergo

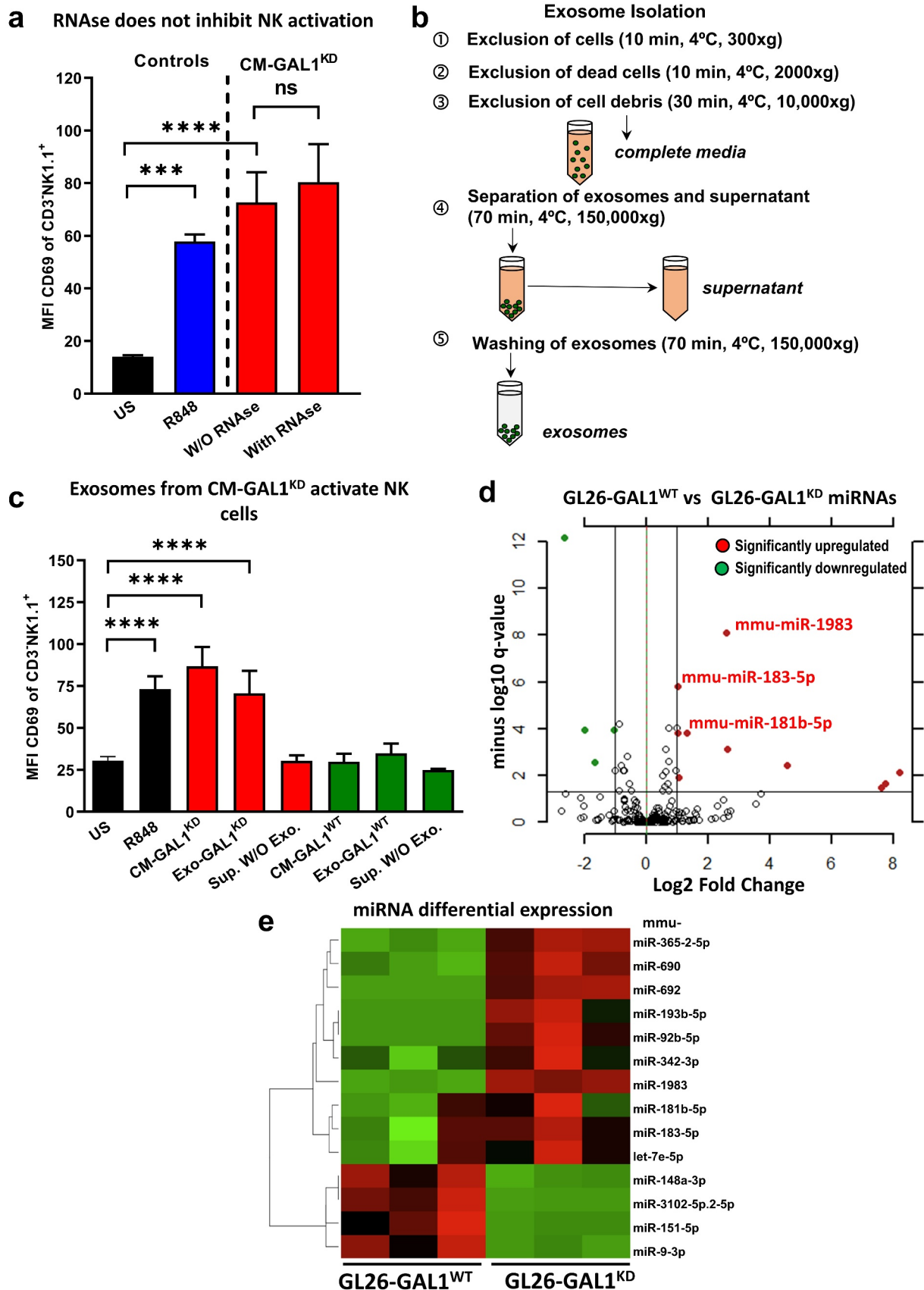


Figure 4. TLR7 ligands are enclosed within exosomes, which show differential miRNA expression. (a) Flow cytometric analysis of CD69 expression on CD3⁺NK1.1⁺ NK cells in the different experimental conditions. CM-GAL1^{KD} pre-treated with RNase at a dose of 5 U/ml for 30 minutes at 37°C and then inactivated with RNase OUT solution used at 40 U/ml. Splenocytes of wt C57BL/6 J mice were then incubated with pre-treated CM-GAL1^{KD} for 18 h to determine the CD69 expression on NK cells. CD69 expression is shown as mean fluorescent intensity (MFI) in the bar graph. Data are represented as mean ± SEM. *p < .05, **p < .01, ***p < .001, and ****p < .0001 versus respective control group (one-way ANOVA). (b) Schematic representation of the protocol used for exosome isolation from media conditioned by GL26-GAL1^{KD} or GL26-GAL1^{WT} glioma cells. (c) Flow cytometric analysis of CD69 expression on CD3⁺NK1.1⁺ NK cells in the different experimental conditions. For the control condition

splenocytes from wt mice (C57BL/6) were incubated with fresh medium (US), or R848, a TLR7 agonist. To assess if exosomes could be transporting the NK-stimulating factor, splenocytes were stimulated with complete conditioned medium (CM-GAL1^{KD} or CM-GAL1^{WT}), or isolated exosomes (Exo-GAL1^{KD} or Exo-GAL1^{WT}), or supernatant depleted of exosomes (Sup W/O Exo.) derived either from GL26-GAL1^{KD} or GL26-GAL1^{WT} cells. Data are represented as mean \pm SEM corresponding to four technical replicates. * $p < .05$, ** $p < .01$, *** $p < .001$, and **** $p < .0001$ versus respective control group (one-way ANOVA). (d) Volcano plot which illustrates differentially expressed (DE) miRNA isolated from exosomes derived from GL26-GAL1^{KD} or GL26-GAL1^{WT} glioma cells. Differentially expressed genes ($n = 14$) were selected by fold change ≥ 2 (\log_2 fold change of ≥ 1 or ≤ -1) and a q-value (FDR corrected p -value) ≤ 0.05 ($-\log_{10}$ FDR of ≥ 1.30103). Data is plotted as $-\log_{10}$ of the false discovery rate (FDR, y-axis) and the \log_2 fold change between the compared groups (\log_2 foldchange, x-axis). Upregulated genes are shown in red dots ($n = 10$) and downregulated genes in green dots ($n = 4$). The FDR-adjusted significance q-values were calculated using a two-sided moderated Student's t-test. (e) Heat map of supervised analysis using Top 50 Variable microRNAs from exosomes derived from GL26-GAL1^{KD} or GL26-GAL1^{WT} glioma conditioned media. Heat map shows miRNA expression pattern within the exosomes. Three biological replicates per group were analyzed. Upregulated genes are represented in red and downregulated genes are represented in green (q-value ≤ 0.05 and fold change ≥ 2). The differential expression of miRNA genes in both conditions is clearly visible.

lysis in response to R848 pre-activated NK cells. These data confirm that activated NK cells mediate glioma killing when stimulated by TLR7 agonists (Figure 5d).

To assess the dose-dependent response of miRNAs, we examined the three miRNAs that had strongest effects, miR-1983, miR-183-5p and miR-181b-5p, at concentrations of 0.01–1 μ M. We also included an unstimulated control group (Plain-media) as well as a positive control group receiving R848 (Resiquimod), a TLR7-specific synthetic agonist. We determined the expression of the activation marker CD69 on CD45⁺CD3⁺NK1.1⁺ gated NK cells in response to miRNAs agonists using flow cytometry. Importantly, splenocytes stimulated with miRNAs (miR-1983, miR-183-5p and miR-181b-5p) resulted in the strong dose-dependent induction of CD69 expression on NK cells (Figure S3B).

miR-1983 stimulates TLR7 signaling through a UGUUU motif

To identify the motif by which miR-1983 binds to TLR7, we mutated various nucleosides within miR-1983, and tested their capacity to stimulate TLR7-mediated NK cell activation (Figure 6a-b and Figure S4A-S4C). We introduced various mutations in the predicted TLR7 binding domain (CUGG) based on its shared presence in miR-1983 and miR-183-5p, the strongest TLR7 agonists. Mutations were introduced in the motif CUGG, keeping the secondary stem-loop structure. We substituted C with U at position 6 (mut-1983-C6U). Similarly, in mut-1983-C6U-U7C, C and U were substituted by U and C at position 6 and 7 and in mut-1983-C6U-U7C-G8C, C, U and G were substituted by U, C and C at position 6, 7, and 8. In the mut-1983-Circ, we mutated miR-1983 at position 1, 2, and 3 into a circular structure keeping the predicted active TLR7 domain (CUGG) (Figure S4B). To our surprise, the mutations implemented did not inhibit NK activation via TLR7 (Figure 6c).

Next we tested the mutations on the 3' side of miR-1983 within the UGUUU motif to identify the TLR7 binding domain. Secondary structures of miR-1983 mutants within the UGUUU motif are shown in Figure S4C. In mut-1983-U14 C, U was substituted with C at position 14 while mut-1983-U14 C-U17G has a substitution to incorporate another UGUU motif shifted toward the 3' side to determine the positional specificity of UGUU within the miRNA. The mutations incorporated at positions 14 and 17 (mut-1983-U14 C-U17G) inhibited the capacity of miR-1983 to stimulate TLR7-mediated activation by 63%. Incorporation of a mutation at position 18 by substituting U by C, keeping the mutation at position 14 and 17 (mut-1983-U14 C-U17G-U18C) reduced

the capacity of miR-1983 to stimulate TLR7-mediated activation by 95% and a comparable inhibition was also observed in the mutant (mut-1983-G15C-U16A-U17 C-U18A) where we mutated nucleosides 15, 16, 17, 18. Altogether, mutagenesis results suggest that the activation site is the sequence UGUUU in the endogenous TLR7 ligand miR-1983. miR-1983 is the most potent in eliciting NK tumor cytotoxicity through binding to TLR7 through its UGUUU motif (Figure 6d). We propose miR-1983 as the endogenous ligand that is secreted by GL26-GAL1^{KD} glioma cells to stimulate TLR-7 mediated NK activation of glioma cell killing.

Discussion

Glioma cells escape cytotoxic T cell recognition by reducing MHC-I expression.^{24,25} Though low MHC-I expression would make cells more sensitive to NK-mediated cytotoxicity, upregulation of Gal-1 expression by glioma cells facilitates NK-immune evasion. Understanding the mechanisms by which gliomas evade NK-mediated cytotoxicity is important to develop new and effective immunotherapies for patients suffering from this devastating disease. Our previous studies in mice and rats uncovered the existence of a powerful innate anti-glioma immune response mediated by NK cells and myeloid cells, which was inhibited by glioma-derived Gal-1.^{4,5} Therefore, the precise mechanisms underlying the regulation of NK-mediated cytotoxicity of glioma cells are the subject of the current study.

Gal-1 is a β -galactoside-binding lectin that promotes glioma malignant behavior. It stimulates angiogenesis,²⁶ and contributes to glioma-mediated immune evasion by modulating anti-tumor immunity.^{27,28} Gal-1 induces T cell apoptosis,^{2,29} inhibits T cell transendothelial migration,³⁰ expands regulatory T cells (Treg),³¹ induces tolerogenic DCs^{32,33} and biases macrophage differentiation toward the protumoral phenotype.^{34,35} Interestingly, in the context of ovarian cancer the anti-tumoral effects of Gal-1 are related to the expression of TLR5.³⁶

Herein we propose the existence of an innate anti-glioma miR1983-TLR7-IFN β -NK circuit in which Gal-1 deficient glioma cells release specific miRNAs within exosomes, which are endogenous TLR7 ligands. These miRNAs activate TLR7 signaling in myeloid cells (pDCs and cDCs). TLR7 downstream signaling through MyD88-IRF5/IRF7 results in secretion of IFN- β , which in turn activates NK cells, which then eradicate glioma tumors (see summary in Figure 7). In the canonical type I IFN-induced signaling pathway, IFNAR engagement activates the receptor-associated protein tyrosine Janus kinase 1 (JAK1) and tyrosine kinase 2 (TYK2), which phosphorylate the

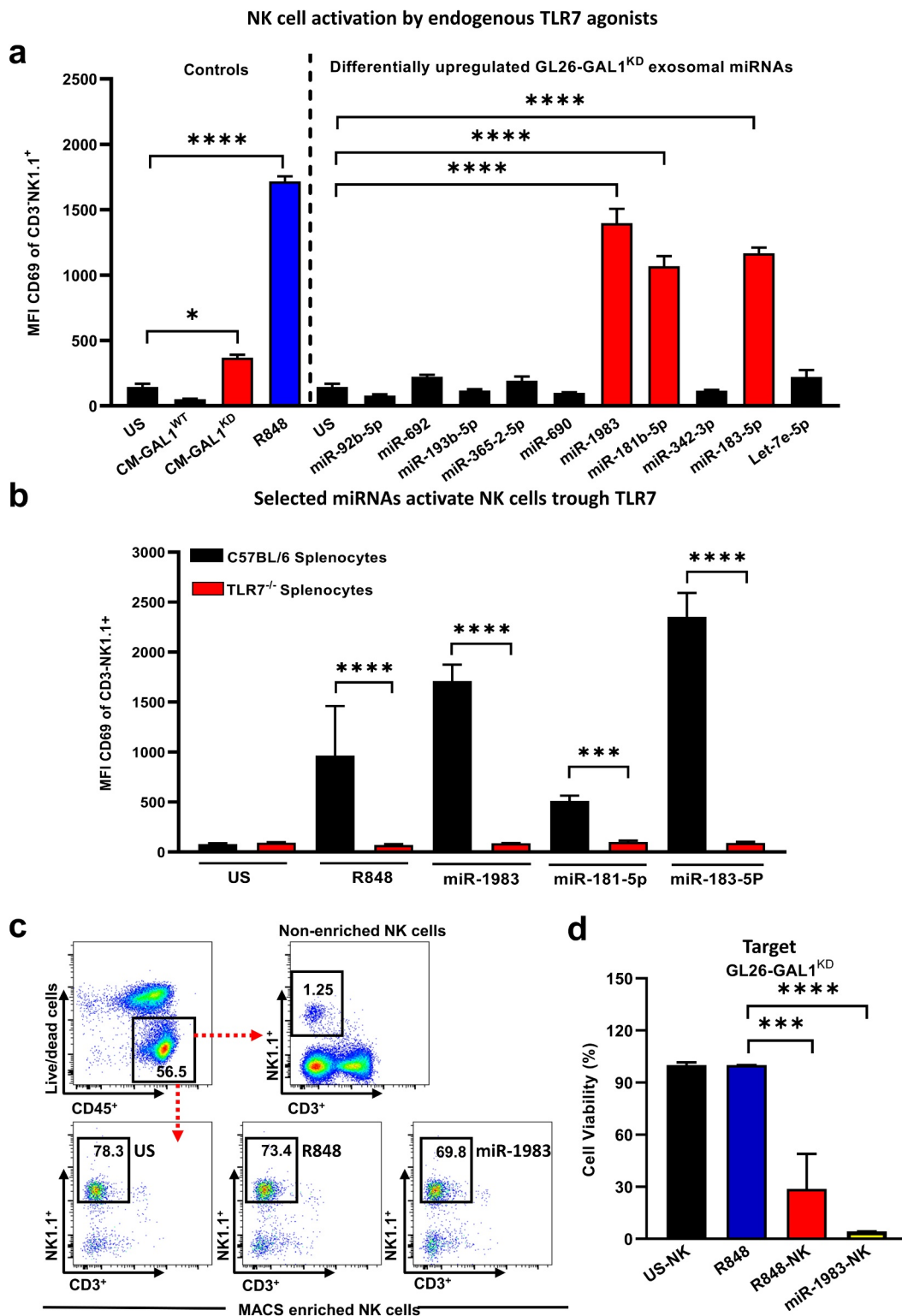


Figure 5. miR-1983 pre-activated NK cells induces GL26-GAL1^{KD} glioma cytotoxicity. (a) Differentially expressed miRNAs from miRNA-seq data were tested for their ability to induce an increase in CD69 expression on NK cells in the whole splenocytes. Splenocytes from C57BL/6 J mice were stimulated with 1 μ M of differentially upregulated miRNAs agonists for 18 h. CD69 expression on CD3⁺NK1.1⁺ NK cells was analyzed using flow cytometry. We also included a comparison between the conditioned media from the galectin-1 expressing (CM-GAL1^{WT}) and deficient cells (CM-GAL1^{KD}). R848, a TLR7 synthetic agonist treated group served as positive control while fresh medium treated served as unstimulated controls (US). Data are represented as mean \pm SEM corresponding to four technical replicates. * p < .05, ** p < .01, *** p < .001, and **** p < .0001 versus respective control group (one-way ANOVA). (b) We considered the three miRNAs that have the strongest effect viz., miR-1983, miR-183-5p, and miR-181b-5p for determining its TLR7 specificity. We also included an unstimulated control group (fresh-media, US) as well as a positive control group receiving R848, a TLR7-specific synthetic agonist. Wt C57BL/6 J splenocytes are shown in black while TLR7^{-/-} splenocytes are shown in red. Data are represented as mean \pm SEM corresponding to four technical replicates. * p < .05, ** p < .01, *** p < .001, and **** p < .0001 versus respective control group (one-way ANOVA). (c) Representative flow cytometry plots illustrating the CD3⁺NK1.1⁺ NK cells in the unsorted population or MACS sorted NK cells. Splenocytes were treated either with fresh medium (US) or R848, or miR-1983 and after 18 h of incubation, MACS-enrichment was performed. (d) GL26-GAL1^{KD} glioma cells were incubated for 72 hr with the MACS-enriched NK cells pretreated either with fresh medium (US-NK) or R848, a TLR7 agonist (R848-NK), or 1 μ M of miR-1983 in DOTAP liposomal transfection reagent. Cell viability was evaluated by performing the CellTiter-Glo (CTG) assay and data are represented as % viability normalized to R848 treated gliomas cells (R848 only).

Data are represented as mean \pm SEM corresponding to three technical replicates. * $p < .05$, ** $p < .01$, *** $p < .001$, and **** $p < .0001$ versus respective control group (one-way ANOVA).

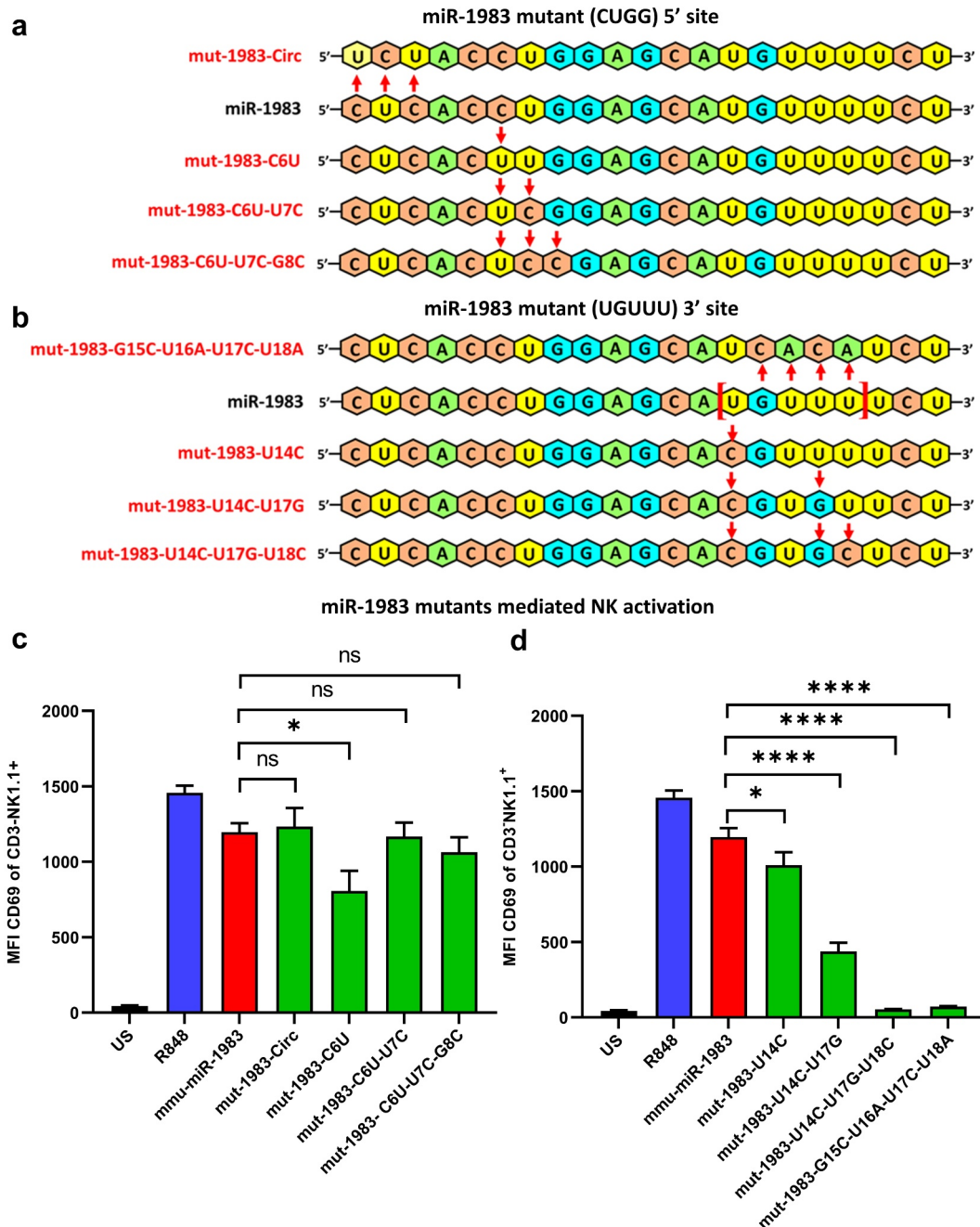


Figure 6. miR-1983 binds to TLR7 through a UGUUU motif to stimulate NK cell activation. To identify the TLR7 binding motif, we mutated various nucleosides within miR-1983, and tested their capacity to stimulate NK cell activation. (a-b) represent the schematics of nucleoside sequence present in parent miR-1983 and corresponding mutations in the CUGG motif toward 5' end (a), and in the UGUUU motif toward 3' end (b). Mutation incorporation site was indicated by the red arrow with respect to the sequence of parent miR-1983. (c-d) Flow cytometric analysis of CD69 expression on CD3⁻NK1.1⁺ NK cells in response to incubation with various miR-1983 mutants. Panel (c) shows the activation in response to CUGG motif mutants while Panel (d) shows the activation in response to UGUUU motif mutants. R848, a TLR7 synthetic agonist treated group served as positive control while fresh medium treated served as unstimulated controls (US). Data are represented as mean \pm SEM corresponding to four technical replicates. * $p < .05$, ** $p < .01$, *** $p < .001$, and **** $p < .0001$ versus respective control group (one-way ANOVA).

transcription factors STAT1 and STAT2.³⁷⁻³⁹ The potential downstream signaling targets of IFN- β in our system, such as JAK/STAT,^{39,40} PI3K/AKT/mTOR,⁴¹ or MAPK/ERK⁴² remain to be assessed in future studies. A relationship between Gal-1 and IFN- β has also been described recently in the context of zymosan A-induced peritonitis.⁴³

The role of TLR7 signaling in the context of glioma has been the subject of several studies. It has been shown that pharmacological stimulation of TLR7 can induce glioma regression.⁴⁴⁻⁴⁶ This is in agreement with our findings that TLR7 signaling in our glioma mouse model is essential for the rejection of GL26-GAL1^{KD} glioma by the innate immune

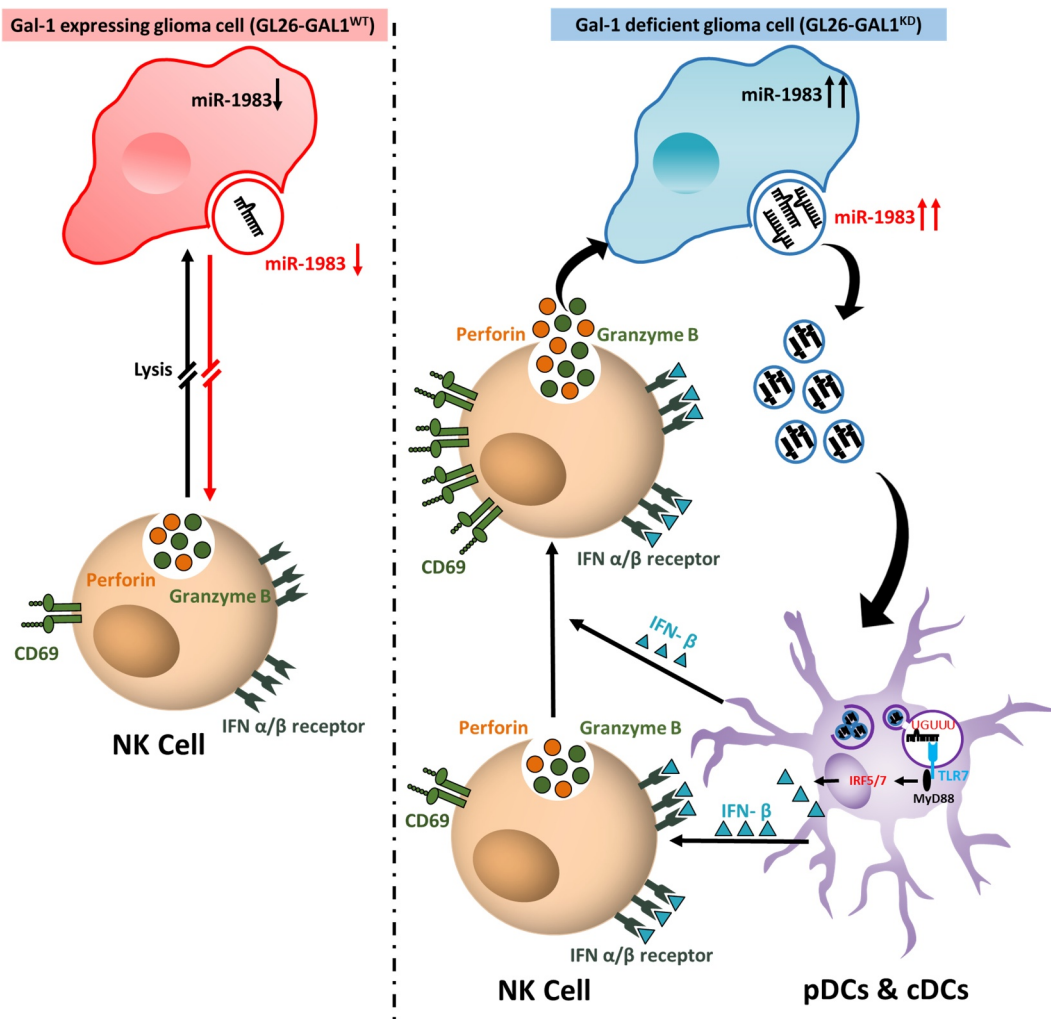


Figure 7. Summary: Schematic of the innate anti-glioma immune circuit mediated by miR-1983-TLR7-NK axis. We discovered the existence of a TLR7-dependent anti-glioma NK-mediated innate immune circuit which is regulated by exosomal miR-1983 and is under the regulation of Gal-1. Right panel shows that GL26-GAL1^{KD} glioma cells release miRNAs within the exosomes that can act as endogenous TLR7 ligands and bind to TLR7 through a UGUUU motif in miR-1983, in a myeloid cell population, such as cDCs and pDCs. TLR7 activation and downstream signaling through MyD88 activates IRF5 and IRF7 which in turn increase release of IFN β . The release of IFN β stimulates NK cells to kill glioma cells by releasing the Perforin and Granzyme B. Left panel shows that galectin-1 expressing GL26-GAL1^{WT} glioma cells produce low level of miR-1983 which makes them unable to trigger the innate immune circuit. Altogether, we found the existence of a novel miR1983-TLR7-IFN β -NK axis which triggers an anti-glioma NK-mediated innate immune circuit in GL26-GAL1^{KD} glioma cells.

system. However, studies demonstrating pro-tumoral effects of TLR7 signaling have been described in the context of other cancers such as lung cancer or pancreatic cancer.^{47–49} Recently, demonstrated that pharmacological administration of let-7b, a TLR-7 agonist, not present in GL26-GAL1^{KD} glioma-derived exosomes, regulates microglial function and suppresses glioma growth through TLR7 signaling induced secretion of TNF- α in both GL261 murine glioma model and *in vitro*.⁵⁰ This shows the potential existence of direct effects of TLR7 signaling on glioma viability, and indirect effects which we demonstrate are mediated by NK-killing.

Addressing the question of TLR7 activation in our model, we demonstrate that only GL26-GAL1^{KD} glioma cells secrete exosomes that contain miRNAs (miR-1983, miR-181b-5p, and miR-183b-5p) which act as endogenous TLR7 ligands. Exosome transfer as a way of intercellular communication has been extensively studied in the context of cancer. Exosome transfer is a process that occurs between cancer cells as well as between cancer cells and the tumor

microenvironment (TME). In particular, cancer cell-derived exosomal miRNAs have been reported to be involved in angiogenesis, tumor progression, metastasis or chemotherapy resistance.^{51–54} The expression signature of exosomal miR-21, miR-222 and miR-124-3p has been proposed as a diagnostic biomarker for glioma patients.⁵⁵ Moreover, it was reported that exosomal transfer of miR-1238 contributes to resistance toward temozolomide in GBM.⁵⁶ However, exosomes have also been reported to have immunogenic properties given the fact that they can contain tumor-specific antigens.^{57,58}

Importantly, sorting of miRNAs into exosomes is a regulated process which we believe is regulated by Gal-1.^{54–59–61} Interestingly, different groups have shown that miRNAs can act as exogenous or endogenous TLR7 ligands in several disease models such as lung cancer, neurodegeneration, systemic lupus erythematosus,^{62–66} though a potential role for TLR7 in NK cell activation in glioma has not yet been described. Though similar TLR7 signaling is operative in human glioma cells,⁵⁰ the exact mechanism by which Gal-1

regulates NK activity in human models remains to be determined.

In our experimental glioma model, the exosomal miRNA landscape is regulated by the expression of Gal-1 in glioma cells. Activation of NK cells reveals that miR-1983 is the most potent endogenous TLR7 ligand and the activation of this circuit results in the eradication of glioma before the activation of anti-tumor adaptive immunity. Antigen-specific adaptive immunity does not peak until 10 to 14-days post-tumor implantation.^{4,67-71} Interestingly, Hasler et al. reported the origin of miR-1983.⁷² They found that Ago-associated small RNA libraries from Lupus autoantigen knockdown cells have one specific pre-tRNA-Ile (Ile-TAT-2-3) fragment that was previously identified in mouse embryonic stem cells and annotated as miR-1983.⁷³ Non-canonical miRNAs can originate from a variety of genomic loci, that comprises small nucleolar RNAs (snoRNAs), transfer RNAs (tRNAs) and introns by bypassing the canonical miRNA biogenesis pathway. By comparing the genomic loci, they further revealed that miR-1983 is highly conserved between mouse and human.⁷² So far only one tRNA-derived miRNA has been described, miR-1983, which is derived from the murine tRNA, IleTAT.⁷³ Whether this is the origin of miR-1983 in glioma cells which is under the control of Gal-1 remains to be determined. We identified the motif UGUUU at the 3' end of the endogenous miR-1983 as the binding sequence to TLR7. Our data are compatible with previous results showing that Guanosine and a succession of 2-3 U's are necessary to stimulate TLR7.⁷⁴⁻⁷⁶

Our data revealed the existence of an innate immune circuit that is initiated by GL26-GAL1^{KD} glioma derived endogenous exosomal miR-1983 that triggers an NK mediated glioma rejection through TLR7 signaling. Importantly, this demonstrates that Gal-1-mediated innate immune suppression acts by altering the miRNA landscape in exosomes to evade NK-immune recognition. Our study identified miR-1983 as an endogenous TLR7 ligand that binds to TLR7 through a UGUUU motif to stimulate TLR7 signaling through IRF5 and IRF7, resulting in IFN β release, and that leads to NK-mediated cytotoxicity. We propose that therapeutic activation of the proposed innate immune circuit could be used to overcome Gal-1-mediated innate immune suppression in gliomas. Based on our findings, we propose that successful immunotherapy for glioma might require not only the inhibition/blocking of adaptive immune suppression by Gal-1, but also stimulate the innate immune activation by endogenous TLR7 ligands.

MATERIALS AND METHODS

Animal Strains

Six to eight week-old female mice of the following transgenic strains were purchased from the Jackson Laboratory: MyD88^{-/-} (B6.129P2(SJL)-MyD88tm1.1Defr/J, Jax# 009088), TLR7^{-/-} (B6.129S1-Tlr7^{tm1Flv}/J, Jax# 008380), TLR5^{-/-} (gifted by Dr. Standiford), TLR2/4^{-/-} (gifted by Dr. Gabriel Nunez), TLR9^{-/-} (C57BL/6 J-Tlr9^{M7Btlr}/Mmjax, Jax# 34329-JAX), NKG2D^{-/-} (B6.Cg-Klrk1tm1Dhr/J, Jax# 022733), Perforin^{-/-} (C57BL/6-Prf1tm1Sdz/J, Jax# 002407), IFN γ R1^{-/-} (B6.129S7-

Ifngr1tm1Agt/J, Jax# 003288), IFN γ ^{-/-} (B6.129S7-Ifngtm1Ts/J, Jax# 002287), BDCA-2-DTR mice (C57BL/6-Tg(CLEC4C-HBEGF)956 Cln/J, Jax# 014176), TNFR^{-/-} (B6.129S-Tnfrsf1b1tm1Imx/J, Jax# 003243), IL1R^{-/-} (B6.129S7-Il1r1tm1Imx/J, Jax# 003245), IL18^{-/-} (B6.129P2-Il18r1tm1Aki/J, Jax#004131), and Rag1^{-/-} (B6.129S7-Rag1tm1Mom/J, Jax# 002216). C57BL/6 mice (Tac# B6-F), Rag2^{-/-} (B6.129S6-Rag2tm1Fwa N12, Tac# RAGN12-F) and Rag2/IL2rg^{-/-} (B10; B6-Rag2tm1Fwa Il2rgtm1Wjl, Tac# 4111-F) were purchased from Taconic. IRF7 mice were generated and kindly provided by Dr. Tadatsugu Taniguchi (University of Tokyo), IRF5 mice were generated and kindly provided by Dr. Tak W. Mak (University of Toronto). The detailed genetics and immunology of the mouse strains are described on the websites <https://www.jax.org> and <https://www.taconic.com/>. All animal experiments were conducted in accordance with procedures approved by the University Committee on Use and Care of Animals and conformed to the policies and procedures of the Unit for Laboratory Animal Medicine at the University of Michigan.

Cell-lines and culture conditions

Galectin-1-expressing murine glioma cells previously described as GL26-Cit-NT while Galectin-1-deficient described as GL26-Cit-galli.⁴ Herein for simplicity, Galectin-1-expressing glioma cells are now described as (GL26-GAL1^{WT}) and Galectin-1-deficient described as (GL26-GAL1^{KD}). Briefly, a plasmid containing the mCitrine transgene (pRSET-B-Citrine) was subcloned into the pCI-neo expression vector backbone to express the mCitrine fluorescent protein constitutively (pCI-neo-mCitrine). After that, the plasmid was used to transfect GL26 cells. To preserve transgene expression, transfected cells were FACS sorted for high mCitrine expression and cultured under G418 selection antibiotic. To create the GL26-Cit-galli cell lines, pLKO.1-puro lentiviral plasmids encoding a Puromycin resistance cassette as well as shRNA hairpin construct specific for rodent Gal-1 (mlgals1, NM 008495) mRNA was purchased from Sigma-Aldrich as part of the RNAi consortium and tested for their ability to knock down gal-1 expression. To confirm the knockdown, a rodent Gal-1 overexpression vector pCMV6-kan/neo-mlgals1 (Origene, cat. no. MC200092) was co-transfected into HEK293 cells with each of the above-mentioned shRNA constructs. The highest degree of Gal-1 knockdown was achieved by RNAi consortium clone TRCN0000011866, which was used to build a second-generation lentiviral vector encoding this mlgals1-specific shRNA (LV-mLgals1-11866i). The GL26-Cit cells were then transduced for 48 to 72 hours with 80 μ L of filtered LV-mLgals1-11866i. To enrich for transduced cells, infected cells were grown under Puromycin selection. The GL26-Cit-NT control cell lines, which also contain the pLKO.1-puro lentiviral expression vector, were created using a similar process, expressing a scrambled shRNA hairpin construct (Mission shRNA, cat. no. SHC002; Sigma-Aldrich). Cells were cultured in Dulbecco Modified Eagle Medium (DMEM) supplemented with 10% fetal bovine serum (FBS), 50 U/ml Penicillin, 50 μ g/ml Streptomycin, 0.3 mg/ml L-glutamine,

3 µg/ml Puromycin and 0.6 mg/ml G418 under humidified conditions in 95% air/5% CO₂ at 37°C.

Flow cytometry antibodies

The following antibodies were used for NK cell analysis: FITC anti-mouse CD3ε (BD Biosciences, Cat# 553062, clone 145–2 C11), APC anti-mouse NK1.1 (eBioscience/Affymetrix, Cat# 17–5941, clone PK136), PerCp-Cy5.5 anti-mouse CD45 (BioLegend, Cat# 103132, clone 30-F11) and PE anti-mouse CD69 (BioLegend, Cat# 104507, clone H12F3). For pDCs analysis we used: PE-anti-mouse CD317 (PDCA-1) (BioLegend, Cat# 127104, clone 129C1), PerCp/Cy5.5 anti-mouse CD45 (BioLegend, Cat# 103132, clone 30-F11), APC anti-mouse CD11c (BioLegend, Cat# 117310, clone N418) and FITC anti-mouse/human CD45R/B220 (BioLegend, Cat# 103206, clone RA3-6B2). For myeloid cells we used: PerCp-Cy5.5 anti-mouse CD11b (BioLegend, Cat# 101228, clone M1/70), APC anti-mouse CD45 (BioLegend, Cat# 103112, clone 30-F11), FITC-anti-mouse Ly6C/Ly6G (Gr-1) (BioLegend, Cat# 108406, clone RB6-8 C5), PB anti-mouse F4/80 (BioLegend, Cat# 123123, clone BM8). For TLR7 expression analysis, we procured PE-anti-mouse TLR7 (BD Biosciences, Cat# 565557, clone A94B10). Exclusion of dead cells from the analysis was done based on staining with LIVE/DEAD™ Fixable Aqua Dead Cell Stain Kit (ThermoFisher Scientific Cat# L34957), or DAPI (4′-diaminophenylindolehydrochloride, ThermoFisher Scientific, Cat# D21490), or fixable viability dye eFluor780 (ThermoFisher Scientific, Cat# 65–0865-14).

Flow cytometry staining

To label surface antigens, cells were washed twice with azide- and serum/protein-free PBS then labeled with the fixable viability dye eFluor780, and incubated for 30 min in the dark at 4°C. Cells were then washed twice with FACS buffer (PBS containing 2% FBS) and nonspecific antibody binding was blocked with anti-mouse CD16/CD32 (BioLegend, Cat# 101302) for 10 min on ice. Cells were centrifuged for 5 min at 4°C and 1,500 rpm and then stained with the following specific primary antibodies mixes for NK1 cells: NK1.1, CD3, CD45, for pDCs and cDCs cells: CD45, CD11c, B220, PDCA-1, and for macrophages: CD45, CD11b, Gr-1, F4/80. After 20 min incubation on ice in the dark, cells were washed twice with FACS buffer. For fixation of samples, cells were centrifuged for 5 min at 4°C and 1,500 rpm, resuspended in 2% PFA, and incubated for 20 min at RT in the dark. Cells were then washed twice with PBS and resuspended in FACS buffer for analysis. For intracellular staining of TLR7, cells were washed twice in PBS/2% FBS and then fixed and permeabilized using the Cytofix/Cytoperm kit (BD Biosciences, Cat# 554714) according to the manufacturer's protocol. Cells were incubated with the anti-TLR7 antibody for 30 min at 4°C in the dark, followed by two washing steps in Perm/Wash buffer. Finally, cells were centrifuged for 5 min at 4°C and 1,500 rpm and resuspended in PBS/2% FBS for analysis. All the samples were acquired on a FACSAria II flow cytometer (BD Biosciences) using FACS-Diva software (BD Biosciences, version 8.0.1). Final data

analysis was done using FlowJo software version 10 (Treestar Inc.). Gating was performed based on Fluorescence minus one (FMO) controls.

Preparation of conditioned medium

For pre-conditioning of culture supernatants, GL26-GAL1^{WT} or GL26-GAL1^{KD} cells were seeded in a 48-well plate at a concentration of 20,000 cell/well in 300 µl DMEM supplemented with 10% fetal bovine serum (FBS), 50 U/ml Penicillin, 50 µg/ml Streptomycin and 0.3 mg/ml L-glutamine. The DMEM culture medium was left on cells for 96 h after seeding before being harvested. Conditioned medium was centrifuged at 1,500 rpm for 5 min at 4°C to remove remaining cell debris, then filtered using Millex-GS syringe 0.22 µm filter (Millipore Sigma, US) before using for further experiments.

Splenocyte isolation and its stimulation with conditioned medium derived from GL26-GAL1^{WT} or GL26-GAL1^{KD} glioma cells

Spleens from 6–10 week old female mice were harvested and homogenized through a 70 µm sterile cell strainer using a 1 ml syringe plunger. Cells were flushed with 15 ml of DMEM+10% FBS to pass through the strainer with minimal cell loss. Cell suspension was transferred into a 15 ml Falcon tube, and then centrifuged at 1500 rpm for 5 min at 4°C and cells were resuspended in 1 ml of RBC lysis buffer (BioLegend, Cat# 420301) and incubate for 2 min on ice, lysis was stopped by adding cold PBS followed by centrifugation at 1500 rpm for 5 min at 4°C. Cells were resuspended in 10 ml of cold PBS containing 10% FBS and filtered through a 70 µm cell strainer. Splenocytes was diluted 1:2 in Trypan blue viability dye (ThermoFisher Scientific, Cat# 15250061) to count the number of viable cells using a hemocytometer. To determine the NK activation, splenocytes of wt mice (C57BL/6) were seeded in a round-bottom 96-well plate at a concentration of 1 × 10⁶ cells/well in 25 µl. Controls received either fresh DMEM or undiluted conditioned medium collected from GL26-GAL1^{WT} or GL26-GAL1^{KD} cells. CM-GAL1^{KD} was diluted either with fresh DMEM or CM-GAL1^{WT} at the ratio of 1:10, 1:100, 1:1000, and 100 µl/well were added to splenocytes. Respective amounts of fresh media were added to each well to reach an equal final volume of 150 µl in all wells.

In vivo immunodepletion and blocking experiments

The following antibodies were intraperitoneally injected to deplete NK cells (per mouse): 200 µg monoclonal anti-mouse NK1.1 on days –2, 1, 5 post-tumor implantation (DPI) (clone PK136, Cat# 16–5941, eBioscience) and equivalent to 200 µg of purified mouse IgG2a, κ isotype control antibody was injected in the control group at the respective days (clone:MG2a-53, Cat# 401502, BioLegend): 25 µl of stock rabbit polyclonal anti-asialo GM1 serum on days –1, 1, 4 DPI (ASGM1, Cat# 986–10001, Wako) and 100 µl of undiluted normal rabbit serum was injected in the control group at the respective days (Life Technologies, Cat# 16120). Depletion of plasmacytoid dendritic cells (pDCs) in BDCA-2-DTR mice was performed by

intraperitoneal injections of 100 ng diphtheria toxin on days -1, 1, 3, 5 DPI.

Immunodepletion of Gr1⁺ or Ly6G⁺ myeloid cells was achieved by intraperitoneal injections of 500 µg monoclonal anti-Gr-1 (BioXCell, Cat# BE0075, clone RB6-85 C) or 600 µg monoclonal anti-Ly6G (BioXCell, Cat# BE0075-1, clone 1A8) antibodies on days -1, 3 DPI. Animals in the control groups received 500 µg/mouse and 600 µg/mouse IgG (Equitech-Bio, Cat# RT60-0100), respectively.

In vivo blocking of the interferon α/β receptor 1 was performed by intraperitoneal injection of 500 µg/mouse monoclonal mouse anti-IFNAR1 antibody (Leinco Technologies, Cat# I-401, Clone: MAR-5A3) on days -1, 0, 1, 2 DPI and 250 µg/mouse on days 4, 6 DPI. Animals in the control group received identical amounts of mouse IgG1 isotype control antibody (Leinco Technologies, Cat# I-536). *In vivo* depletion of type I Interferon, IFN-α and IFN-β was achieved by injecting the purified *in vivo* GOLD™ functional grade monoclonal anti-mouse IFN-α (Leinco technologies, Cat# I-1183-5.0, Clone: TIF-3 C5), anti-mouse IFN-β (Leinco technologies, Cat# I-439-5.0, Clone: MIB-5E9.1) intraperitoneally at a dose of 250 µg/mouse on days -1, 0, 1, 3, 5 DPI. Control mice received identical amounts of purified *in vivo* GOLD™ functional grade Armenian hamster IgG Isotype Control (Leinco technologies, Cat# I-140-5.0, Clone: PIP). For neutralization of IL-12 *in vivo*, mice were subjected to intraperitoneal injections of 500 µg of monoclonal anti-mouse IL12p40 antibody (BioXCell, Cat# BE0051, clone C17.8) on days 0, 1, 3, 5 DPI. Mice in the control group were treated with 500 µg rat IgG2a isotype control antibody (BioXCell, Cat# BE0089, clone 2A3).

Intracranial tumor implantation and tissue processing

For tumor growth analysis, intracranial tumor implantation was performed as previously described.⁷⁷⁻⁷⁹ Briefly, 6–25 weeks old mice were implanted with 3.0×10^4 GL26-GAL1^{KD} cells into the right striatum of the brain with a 22 G Hamilton syringe using the following coordinates +1.00 mm anterior, 2.5 mm lateral, and 3 mm deep. Mice were transcardially perfused on day 7 after tumor implantation. Mice were anesthetized by intraperitoneal injection of ketamine hydrochloride and xylazine hydrochloride in sterile 0.9% saline. Using a peristaltic pump, mice were transcardially perfused with oxygenated and heparinized Tyrode's solution followed by 4% Paraformaldehyde (PFA) solution in PBS (pH = 7.4). Brains were harvested and post-fixed in 4% PFA overnight at 4°C.

Quantification of tumor size

PFA-fixed mouse brains were coronally sectioned into 50 µm thick sections using a vibratome (Leica VT1000S, Leica) and placed consecutively into six wells (in a 6-well tissue culture plate containing 2 ml/of PBS with 0.01% sodium azide in each well) as described by us previously.^{4,5} Therefore, each well contains representative sections (i.e., 1/6th of the whole

tumor). For each mouse, sections of one well were mounted on glass slides and cover-slipped using Prolong gold antifade reagent (Thermo Fisher Scientific, Cat# P36931). Brain sections containing mCitrine fluorescence of GL26-GAL1^{KD} tumors were imaged at 4X magnification using epifluorescence microscopy (Zeiss Axioplan2, Carl Zeiss MicroImaging). For quantification of tumor size, images of brain sections exhibiting fluorescence were quantified using ImageJ software (National Institute of Health, Bethesda, MD), using Otsu threshold, and tumor size was determined in pixels using the following steps: I. Image > Type > 8-bit, II. Image > Adjust > Threshold > Apply, III. Process > Binary > Make Binary, and IV. Analyze > Measure. The area output of each measurement was then added to afford an estimate of overall tumor size. Additionally, representative images of tumor size for each mouse were obtained employing tiles scanning and confocal microscopy (Carl Zeiss MIC-System).

Enrichment of NK cells from splenocytes using MACS

Splenocytes were isolated as described above. Cells were centrifuged for 5 min at 4°C and 1,500 rpm and cells were resuspended in PBS containing 1 mM EDTA and 2% FBS at a concentration of 1×10^8 cells/ml. Magnetic enrichment of NK cells was achieved by negative selection using EasySep mouse NK cell isolation kit (Cat# 19855, Stemcell Technologies). Briefly, 50 µl/ml EasySep mouse NK cell isolation cocktail was added to the cell suspension and incubated for 10 min at room temperature. EasySep Streptavidin RapidSpheres were vortexed for 30s and 100 µl/ml RapidSpheres were added to the cell suspension and incubated for 5 min at room temperature. PBS/2% FBS/1 mM EDTA was then added to bring the total volume to 2.5 ml and placed into the magnet. After 5 min of incubation, the magnet holding the tube was inverted and the NK cell-containing fraction was collected. The remaining cells were again resuspended in 2.5 ml PBS/2% FBS/1 mM EDTA to collect the remaining NK cells and placed into the magnet for 5 min and the NK cells containing fraction was again collected and combined with the first NK cell fraction. Enriched NK cells were then centrifuged at 4°C for 5 min at 1,500 rpm, supernatant was carefully removed and cells were resuspended in DMEM media supplemented with 10% FBS, 50 U/ml Penicillin, and 50 µg/ml Streptomycin. Purity of MACS-enriched NK cells was then confirmed by flow cytometry.

Isolation of exosomes from conditioned medium

GL26-GAL1^{WT} and GL26-GAL1^{KD} cells were used to analyze the miRNA profile within exosomes released into the media. 6×10^5 cells were seeded in 100 mm dish with the corresponding media and incubated for 4 days in a 37°C incubator (95% air and 5% CO₂). Then, media was collected and centrifuged to precipitate exosomes. Briefly, media was first centrifuged for 10 minutes at 300xg, 4°C, without breaks and then centrifuged 10 minutes at 2000xg, 4°C, without breaks to eliminate cells and dead cells. Then media was ultra-centrifuged for

30 minutes at 10000xg at 4°C to eliminate cell debris, followed by two centrifugations of 70 minutes at 150000xg at 4°C to collect the exosome fraction. Exosome fractions were maintained at -80°C for 24 hours until miRNA-isolation.

miRNA isolation from exosomes and RNA-sequencing analysis

Exosome fractions were defrosted on ice and miRNA was isolated using the miRNeasy Serum/Plasma Advanced Kit (QIAGEN). Briefly, 600 µl of each exosome fraction was transferred into a 2 ml tube, resuspended with 180 µl of RPL buffer, and incubated for 3 minutes at room temperature. Then, 20 µl buffer RPP was added and tubes were vortexed for 20 seconds, incubated for 3 minutes, and centrifuged at 12000 x g for 3 min at room temperature to pellet the precipitate. Supernatants were mixed with an equal volume of isopropanol and transferred to an RNeasy UCP MinElute column, and centrifuged for 15 s at ≥8000 x g. Column was washed with 700 µl of buffer RWT and centrifuged for 15 s at ≥8000 x g. After, 500 µl of buffer RPE was added to the spin column and centrifuged for 15 s at ≥8000 x g. Column was rinsed with 500 µl of 80% ethanol and centrifuged for 2 min at ≥8000 x g. Finally, miRNA was eluted with 20 µl RNase-free water preheated at 37 °C.

miRNA-Sequencing analysis was performed by NORGE Biotek Corporation (Thorold, ON, Canada). Prior to library preparation, RNA used for Small-RNA-Seq was analyzed for quality control (QC) to ensure a sufficient sample amount and purity. 1 µl of RNA was used in a 20 µl RiboGreen Assay and 1 µl of RNA was used in housekeeping miR-21 RT-PCR for quantification of RNA.

For analysis of miRNA, data were filtered at a minimum of 5 counts (CPM cutoff value to 6.34 in ≥ 3 replicates) and normalized using trimmed mean of M-values (TMM) normalization method as described by.^{80,81} This method takes into account variations in sequencing depth and library size. TMM normalized counts were used for miRNA differential expression analysis was performed to predict relative miRNA expression variations between GL26-GAL1^{WT} vs GL26-GAL1^{KD} groups. EdgeR statistical software package was used for DE analysis and Benjamini-Hochberg method was used adjusting the false discovery rate (FDR). DE cutoff was determined by more than a 2-fold difference at an FDR of ≤ 0.05. DE expression analysis was used to generate Volcano plot graph, Heat map 2D matrix representing hierarchal clustering of miRNAs and samples and Principal component analysis (PCA) to generate sample clustering plot based on miRNAs with the highest variation across all samples.

Synthetic miRNA mimics

RNA oligo-ribonucleotides were modified and synthesized by Integrated DNA Technologies, Inc. (IDT). During modification, the phosphorothioate (PS) bond represented by 'r_*' was introduced throughout the entire oligo-ribonucleotides which substitutes a sulfur atom for non-bridging oxygen in the phosphate backbone of an oligo-ribonucleotide. This modification makes the inter-nucleotide linkage resistant to both

exonuclease and endonuclease attack and provides enhanced stability to the synthesized oligo-ribonucleotide. The details of the mature sequences with the represented PS bond, miRBase accession number, GU, AU, and U content of each differentially upregulated miRNA is shown in Supplemental Table S2.

NK stimulation with synthetic miRNA mimics identified by miRNA-sequencing

To assess the NK stimulation in response to miRNAs agonist, splenocytes of wt mice (C57BL/6) or TLR7 knockout mice were seeded in a round-bottom 96-well plate at a concentration of 1×10^6 cells/well in 100 µl and treated with the respective miRNA agonist. N-[1-(2,3-Dioleoyloxy)propyl]-N,N,N-trimethylammonium methyl-sulfate (DOTAP) cationic liposomal transfection reagent (#11202375001, Roche Diagnostics) was used for the delivery of miRNAs (listed in Table1). Briefly, 1 µM of miRNA mimics in 25 µl of Nuclease Free Water (NFW) or R848 (TLR7/8 agonist, 10 µg/ml, Invitrogen, Cat# tlr-r848) were complexed with 5 µg of DOTAP in 25 µl of NFW. The transfection mixture was gently mixed by pipetting the mixture several times and incubate for 15 min at room temperature. After the formation of complexes, 50 µl of DMEM-wt media supplemented with Exosome-depleted FBS, One-Shot format (#A27208-03, GibcoTM) was added and pipetted gently to mix it. The splenocytes with the DOTAP complexed miRNA mixture were cultured for 18 hr and analyzed for NK cell activation employing FACS as described elsewhere.

miR-1983 stimulated MACS enriched NK cell cytotoxicity

For NK cell-mediated cytotoxicity studies, splenocytes were treated with DOTAP complexed miR-1983 and R848 as described above. After 18 hr of incubation, splenocytes were harvested and MACS enrichment of NK cells was performed as described above. The purity of NK cells was determined by employing FACS. Co-cultured 2×10^4 MACS enriched-NK cells with 5×10^3 GL26-GAL1^{KD} glioma cells at E: T ratio 4: 1. After 72 hr, Cell viability was analyzed by performing the CellTiter-Glo Assay. Briefly, CellTiter-Glo reagent equal to the volume of cell culture medium present in each well was added and plate was put on an orbital shaker to induce cell lysis. After cell lysis, plate was incubated at room temperature for 10 min to stabilize luminescent signal and luminescence was recorded on EnSpire Multimode Plate Reader by PerkinElmer, Inc.

Statistical analysis

Statistical tests used for particular experiments are specified in the results section or the respective figure legends. Unpaired Student's t-test or one-way analysis of variance (ANOVA), followed by Tukey's multiple comparisons posttest were utilized for comparing experimental groups with controls from flow cytometry analysis and NK-cell functional assays. EdgeR statistical software package was used for differential expression analysis and Benjamini-Hochberg method was used adjusting the false discovery rate (FDR), and differentially expressed genes were considered when $FDR \leq 0.05$, and fold change $\geq \pm 2.0$. All quantitative data are

presented as mean \pm SEM from at least three independent experiments. *P*-values of ≤ 0.05 were considered significant. All other analyses were conducted using GraphPad Prism (GraphPad Software Inc, version 7 and version 8).

SUPPLEMENTAL INFORMATION

All relevant data are included in the Supplemental Information.












Acknowledgments

We thank all members of our laboratory for advice and comments on this work.

Funding

This work was supported by the National Institutes of Health, National Institute of Neurological Disorders and Stroke (NIH/NINDS) grants: R37-NS094804, R01-NS105556, R21-NS107894, R21-NS091555, R01-NS074387 to M.G.C.; National Institute of Neurological Disorders and Stroke (NIH/NINDS) grants: R01-NS076991, R01-NS096756, R01-NS082311 to P.R.L.; National Institute of Biomedical Imaging and Bioengineering (NIH/NIBI): R01-EB022563; National Cancer Institute (NIH/NCI) U01CA224160; Rogel Cancer Center at The University of Michigan G023089 to M.G.C.; Ian's Friends Foundation grant G024230; Leah's Happy Hearts Foundation grant G013908; Pediatric Brain Tumor Foundation grant G023387 and ChadTough Foundation grant G023419 to P.R.L.; RNA Biomedicine grant: F046166 to M.G.C.; Health and Human Services, National Institutes of Health, UL1TR002240 to Michigan Institute for Clinical and Health Research (MICHHR); Postdoctoral Translational Scholars Program (PTSP) Project F049768 to A.C., and NIH/NCI T32-CA009676 Post-Doctoral Fellowship to D.S. and M.S.A.

ORCID

Diana Shah  <http://orcid.org/0000-0002-1140-2078>
 Andrea Comba  <http://orcid.org/0000-0002-3398-5753>
 Syed M. Faisal  <http://orcid.org/0000-0002-3968-7810>
 Padma Kadiyala  <http://orcid.org/0000-0002-3273-9905>
 Gregory J. Baker  <http://orcid.org/0000-0002-5196-3961>
 Mahmoud S. Alghamri  <http://orcid.org/0000-0002-8018-7674>
 Robert Doherty  <http://orcid.org/0000-0001-9307-7995>
 Daniel Zamler  <http://orcid.org/0000-0003-0375-8119>
 Gabriel Nuñez  <http://orcid.org/0000-0002-6529-2695>
 Maria G. Castro  <http://orcid.org/0000-0003-2237-2756>
 Pedro R. Lowenstein  <http://orcid.org/0000-0002-8427-4409>

AUTHOR CONTRIBUTIONS

D.S., A.C., S.M.F., M.G.C., and P.R.L. designed the experiments. D.S., A.C., S.M.F., P.K., G.J.B., M.S.A., R.D., and D.Z. performed the experiments. G.N., P.R.L., and M.G.C. provided materials. D.S., A.C., S.M.F., M.G.C., and P.R.L. wrote the paper with assistance from all authors. PRL and MGC supervised the project. All authors read the final version and approved the manuscript.

DECLARATION OF INTERESTS

All authors declare no potential conflicts of interest.

References

- Zhang AS, Ostrom QT, Kruchko C, Rogers L, Peereboom DM, Barnholtz-Sloan JS. Complete prevalence of malignant primary brain tumors registry data in the United States compared with other common cancers, 2010. *Neuro Oncol.* 2017;19(5):726–735. doi:10.1093/neuonc/now252.
- Perillo NL, Pace KE, Seilhamer JJ, Baum LG. Apoptosis of T cells mediated by galectin-1. *Nature.* 1995;378(6558):736–739. doi:10.1038/378736a0.
- Rubinstein N, Alvarez M, Zwirner NW, Toscano MA, Ilarregui JM, Bravo A, Mordoh J, Fainboim L, Podhajcer OL, Rabinovich GA. Targeted inhibition of galectin-1 gene expression in tumor cells results in heightened T cell-mediated rejection; A potential mechanism of tumor-immune privilege. *Cancer Cell.* 2004;5(3):241–251. doi:10.1016/S1535-6108(04)00024-8.
- Baker GJ, Chockley P, Yadav VN, Doherty R, Ritt M, Sivaramakrishnan S, Castro MG, Lowenstein PR. Natural killer cells eradicate galectin-1-deficient glioma in the absence of adaptive immunity. *Cancer Res.* 2014;74(18):5079–5090. doi:10.1158/0008-5472.CAN-14-1203.
- Baker GJ, Chockley P, Zamler D, Castro MG, Lowenstein PR. Natural killer cells require monocytic Gr-1 + /CD11b + myeloid cells to eradicate orthotopically engrafted glioma cells. *Oncoimmunology.* 2016;5(6):e1163461. doi:10.1080/2162402X.2016.1163461.
- Crane CA, Austgen K, Haberthur K, Hofmann C, Moyes KW, Avanesyan L, Fong L, Campbell MJ, Cooper S, Oakes SA, et al. Immune evasion mediated by tumor-derived lactate dehydrogenase induction of NKG2D ligands on myeloid cells in glioblastoma patients. *Proc Natl Acad Sci U S A.* 2014;111(35):12823–12828. doi:10.1073/pnas.1413933111.
- Deng W, Gowen BG, Zhang L, Wang L, Lau S, Iannello A, Xu J, Rovis TL, Xiong N, Raulet DH. A shed NKG2D ligand that promotes natural killer cell activation and tumor rejection. *Science.* 2015. 136–139. doi: 10.1126/science.1258867.
- Diefenbach A, Jamieson AM, Liu SD, Shastri N, Raulet DH. Ligands for the murine NKG2D receptor: expression by tumor cells and activation of NK cells and macrophages. *Nat Immunol.* 2000;1(2):119–126. doi:10.1038/77793.
- Bottino C, Castriconi R, Moretta L, Moretta A. Cellular ligands of activating NK receptors. *Trends Immunol.* 2005;26(4):221–226. doi:10.1016/j.it.2005.02.007.
- Lanier LL. NK cell recognition. *Annu Rev Immunol.* 2005;23(1):225–274. doi:10.1146/annurev.immunol.23.021704.115526.
- Karimi K, Boudreau JE, Fraser K, Liu H, Delanghe J, Gaudie J, Xing Z, Bramson JL, Wan Y. Enhanced Antitumor Immunity Elicited by Dendritic Cell Vaccines Is a Result of Their Ability to Engage Both CTL and IFN γ -producing NK Cells. *Mol Ther.* 2008;16:411–418.
- Keppel MP, Saucier N, Mah AY, Vogel TP, Cooper MA. Activation-specific metabolic requirements for NK Cell IFN- γ production. *J Immunol.* 2015;194(4):1954–1962. doi:10.4049/jimmunol.1402099.
- Barton GM, Medzhitov R. Toll-like receptor signaling pathways. *Science.* 2003;300(5625):1524–1525. doi:10.1126/science.1085536.
- Fitzgerald KA, Kagan JC. Toll-like Receptors and the Control of Immunity. *Cell.* 2020;180(6):1044–1066. doi:10.1016/j.cell.2020.02.041.
- Satoh T, Akira S. Toll-Like Receptor Signaling and Its Inducible Proteins. *Microbiol Spectr.* 2016;4(6):4. doi:10.1128/microbiolspec.MCHD-0040-2016.
- Takeda K, Akira S. Toll-like receptors. *Curr Protoc Immunol.* 2015;109:14 12 11–14 12 10.
- Beutler BA. TLRs and innate immunity. *Blood.* 2009;113(7):1399–1407. doi:10.1182/blood-2008-07-019307.
- Kawai T, Akira S. TLR signaling. *Cell Death Differ.* 2006;13(5):816–825. doi:10.1038/sj.cdd.4401850.
- Kawasaki T, Kawai T. Toll-like receptor signaling pathways. *Front Immunol.* 2014;5:461. doi:10.3389/fimmu.2014.00461.
- Takeda K, Akira S. TLR signaling pathways. *Semin Immunol.* 2004;16(1):3–9. doi:10.1016/j.smim.2003.10.003.
- Curtin JF, King GD, Barcia C, Liu C, Hubert FX, Guillonau C, Josien R, Anegón I, Lowenstein PR, Castro MG. Fms-like tyrosine kinase 3 ligand recruits plasmacytoid dendritic cells to the brain.

- J Immunol. 2006;176(6):3566–3577. doi:10.4049/jimmunol.176.6.3566.
22. Curtin JF, Liu N, Candolfi M, Xiong W, Assi H, Yagiz K, Edwards MR, Michelsen KS, Kroeger KM, Liu C, *et al.* HMGB1 mediates endogenous TLR2 activation and brain tumor regression. *PLoS Med.* 2009;6(1):e10. doi:10.1371/journal.pmed.1000010.
 23. Heil F, Hemmi H, Hochrein H, Ampenberger F, Kirschning C, Akira S, Lipford G, Wagner H, Bauer S. Species-specific recognition of single-stranded RNA via toll-like receptor 7 and 8. *Science.* 2004;303(5663):1526–1529. doi:10.1126/science.1093620.
 24. Bubenik J. MHC class I down-regulation: tumour escape from immune surveillance? (review). *Int J Oncol.* 2004;25:487–491.
 25. Zagzag D, Salnikow K, Chiriboga L, Yee H, Lan L, Ali MA, Garcia R, Demaria S, Newcomb EW. Downregulation of major histocompatibility complex antigens in invading glioma cells: stealth invasion of the brain. *Lab Invest.* 2005;85(3):328–341. doi:10.1038/labinvest.3700233.
 26. Rorive S, Belot N, Decaestecker C, Lefranc F, Gordower L, Micik S, Maurage CA, Kaltner H, Ruchoux MM, Danguy A, *et al.* Galectin-1 is highly expressed in human gliomas with relevance for modulation of invasion of tumor astrocytes into the brain parenchyma. *Glia.* 2001;33(3):241–255. doi:10.1002/1098-1136(200103)33:3<241::AID-GLIA1023>3.0.CO;2-1.
 27. Verschuere T, De Vleeschouwer S, Lefranc F, Kiss R, Van Gool SW. Galectin-1 and immunotherapy for brain cancer. *Expert Rev Neurother.* 2011;8(4):533–543. doi:10.1586/ern.11.40.
 28. Verschuere T, Toelen J, Maes W, Poirier F, Boon L, Tousseyn T, Mathivet T, Gerhardt H, Mathieu V, Kiss R, *et al.* Glioma-derived galectin-1 regulates innate and adaptive antitumor immunity. *Int J Cancer.* 2014;8(4):873–884. doi:10.1002/ijc.28426.
 29. Toscano MA, Bianco GA, Ilarregui JM, Croci DO, Correale J, Hernandez JD, Zwirner NW, Poirier F, Riley EM, Baum LG, *et al.* Differential glycosylation of TH1, TH2 and TH-17 effector cells selectively regulates susceptibility to cell death. *Nat Immunol.* 2007;8(8):825–834. doi:10.1038/ni1482.
 30. He J, Baum LG. Endothelial cell expression of galectin-1 induced by prostate cancer cells inhibits T-cell transendothelial migration. *Lab Invest.* 2006;86(6):578–590. doi:10.1038/labinvest.3700420.
 31. Dalotto-Moreno T, Croci DO, Cerliani JP, Martinez-Allo VC, Dergan-Dylon S, Mendez-Huergo SP, Stupirski JC, Mazal D, Osinaga E, Toscano MA, *et al.* Targeting galectin-1 overcomes breast cancer-associated immunosuppression and prevents metastatic disease. *Cancer Res.* 2013;73(3):1107–1117. doi:10.1158/0008-5472.CAN-12-2418.
 32. Ilarregui JM, Croci DO, Bianco GA, Toscano MA, Salatino M, Vermeulen ME, Geffner JR, Rabinovich GA. Tolerogenic signals delivered by dendritic cells to T cells through a galectin-1-driven immunoregulatory circuit involving interleukin 27 and interleukin 10. *Nat Immunol.* 2009;10(9):981–991. doi:10.1038/ni1772.
 33. Ilarregui JM, Rabinovich GA. Tolerogenic dendritic cells in the control of autoimmune neuroinflammation: an emerging role of protein-glycan interactions. *Neuroimmunomodulation.* 2010;17:157–160.
 34. Correa SG, Sotomayor CE, Aoki MP, Maldonado CA, Rabinovich GA. Opposite effects of galectin-1 on alternative metabolic pathways of L-arginine in resident, inflammatory, and activated macrophages. *Glycobiology.* 2003;13(2):119–128. doi:10.1093/glycob/cwg010.
 35. Starossom SC, Mascanfroni ID, Imitola J, Cao L, Raddassi K, Hernandez SF, Bassil R, Croci DO, Cerliani JP, Delacour D, *et al.* Galectin-1 deactivates classically activated microglia and protects from inflammation-induced neurodegeneration. *Immunity.* 2012;37(2):249–263. doi:10.1016/j.immuni.2012.05.023.
 36. Rutkowski MR, Stephen TL, Svoronos N, Allegranza MJ, Tesone AJ, Perales-Puchalt A, Brenicova E, Escovar-Fadul X, Nguyen JM, Cadungog MG, *et al.* Microbially driven TLR5-dependent signaling governs distal malignant progression through tumor-promoting inflammation. *Cancer Cell.* 2015;27(1):27–40. doi:10.1016/j.ccell.2014.11.009.
 37. Levy DE, Darnell JE. Stats: transcriptional control and biological impact. *Nat Rev Mol Cell Biol.* 2002;3(9):651–662. doi:10.1038/nrm909.
 38. Medrano RFV, Hunger A, Mendonca SA, Barbuto JAM, Strauss BE. Immunomodulatory and antitumor effects of type I interferons and their application in cancer therapy. *Oncotarget.* 2017;8(41):71249–71284. doi:10.18632/oncotarget.19531.
 39. Stark GR, Darnell JE, Jr. The JAK-STAT pathway at twenty. *Immunity.* 2012;36(4):503–514. doi:10.1016/j.immuni.2012.03.013.
 40. Nan Y, Wu C, Zhang YJ. Interplay between Janus Kinase/Signal Transducer and Activator of Transcription Signaling Activated by Type I Interferons and Viral Antagonism. *Front Immunol.* 2017;8:1758.
 41. Weichhart T, Saemann MD. The PI3K/Akt/mTOR pathway in innate immune cells: emerging therapeutic applications. *Ann Rheum Dis.* 2008 Suppl;67(3):iii70–74. doi:10.1136/ard.2008.098459.
 42. Janovec V, Aouar B, Font-Haro A, Hofman T, Trejbalova K, Weber J, Chaperot L, Plumas J, Olive D, Dubreuil P, *et al.* The MEK1/2-ERK Pathway Inhibits Type I IFN Production in Plasmacytoid Dendritic Cells. *Front Immunol.* 2018;9:364. doi:10.3389/fimmu.2018.00364.
 43. Yaseen H, Butenko S, Polishuk-Zotkin I, Schiff-Zuck S, Perez-Saez JM, Rabinovich GA, Ariel A. Galectin-1 Facilitates Macrophage Reprogramming and Resolution of Inflammation Through IFN- β . *Front Pharmacol.* 2020;11:901. doi:10.3389/fphar.2020.00901.
 44. Dumitru CD, Antonysamy MA, Gorski KS, Johnson DD, Reddy LG, Lutterman JL, Piri MM, Proksch J, McGurran SM, Egging EA, *et al.* NK1.1+ cells mediate the antitumor effects of a dual Toll-like receptor 7/8 agonist in the disseminated B16-F10 melanoma model. *Cancer Immunol Immunother.* 2009;58(4):575–587. doi:10.1007/s00262-008-0581-7.
 45. Stathopoulos A, Pretto C, Devillers L, Pierre D, Hofman FM, Kruse C, Jadus M, Chen TC, Schijns VE. Development of immune memory to glial brain tumors after tumor regression induced by immunotherapeutic Toll-like receptor 7/8 activation. *Oncoimmunology.* 2012;1(3):298–305. doi:10.4161/onci.19068.
 46. Xiong Z, Ohlfest JR. Topical imiquimod has therapeutic and immunomodulatory effects against intracranial tumors. *J Immunother.* 2011;34(3):264–269. doi:10.1097/CJI.0b013e318209eed4.
 47. Chatterjee S, Crozet L, Damotte D, Iribarren K, Schramm C, Alifano M, Lupo A, Cherfils-Vicini J, Goc J, Katsahian S, *et al.* TLR7 promotes tumor progression, chemotherapy resistance, and poor clinical outcomes in non-small cell lung cancer. *Cancer Res.* 2014;74(18):5008–5018. doi:10.1158/0008-5472.CAN-13-2698.
 48. Cherfils-Vicini J, Platonova S, Gillard M, Laurans L, Validire P, Caliendo R, Magdeleinat P, Mami-Chouaib F, Dieu-Nosjean MC, Fridman WH, *et al.* Triggering of TLR7 and TLR8 expressed by human lung cancer cells induces cell survival and chemoresistance. *J Clin Invest.* 2010;120(4):1285–1297. doi:10.1172/JCI36551.
 49. Eigenbrod T, Dalpke AH. TLR7 inhibition: a novel strategy for pancreatic cancer treatment? *JAKSTAT.* 2013;2(1):e23011. doi:10.4161/jkst.23011.
 50. Buonfiglioli A, Efe IE, Guneykaya D, Ivanov A, Huang Y, Orłowski E, Kruger C, Deisz RA, Markovic D, Fluh C, *et al.* let-7 MicroRNAs Regulate Microglial Function and Suppress Glioma Growth through Toll-Like Receptor 7. *Cell Rep.* 2019;29(11):3460–3471 e3467. doi:10.1016/j.celrep.2019.11.029.
 51. Kulkarni B, Kirave P, Gondaliya P, Jash K, Jain A, Tekade RK, Kalia K. Exosomal miRNA in chemoresistance, immune evasion, metastasis and progression of cancer. *Drug Discov Today.* 2019;24(10):2058–2067. doi:10.1016/j.drudis.2019.06.010.
 52. Liu X, Lu Y, Xu Y, Hou S, Huang J, Wang B, Zhao J, Xia S, Fan S, Yu X, *et al.* Exosomal transfer of miR-501 confers doxorubicin resistance and tumorigenesis via targeting of BLID in gastric cancer. *Cancer Lett.* 2019;459:122–134. doi:10.1016/j.canlet.2019.05.035.

53. Lucero R, Zappulli V, Sammarco A, Murillo OD, Cheah PS, Srinivasan S, Tai E, Ting DT, Wei Z, Roth ME, *et al.* Glioma-Derived miRNA-Containing Extracellular Vesicles Induce Angiogenesis by Reprogramming Brain Endothelial Cells. *Cell Rep.* 2020;30(7):2065–2074 e2064. doi:10.1016/j.celrep.2020.01.073.
54. Wang M, Yu F, Ding H, Wang Y, Li P, Wang K. Emerging Function and Clinical Values of Exosomal MicroRNAs in Cancer. *Mol Ther Nucleic Acids.* 2019;16:791–804. doi:10.1016/j.omtn.2019.04.027.
55. Santangelo A, Imbruce P, Gardenghi B, Belli L, Agushi R, Tamanini A, Munari S, Bossi AM, Scambi I, Benati D, *et al.* A microRNA signature from serum exosomes of patients with glioma as complementary diagnostic biomarker. *J Neurooncol.* 2018;136(1):51–62. doi:10.1007/s11060-017-2639-x.
56. Yin J, Zeng A, Zhang Z, Shi Z, Yan W, You Y. Exosomal transfer of miR-1238 contributes to temozolomide-resistance in glioblastoma. *EBioMedicine.* 2019;42:238–251. doi:10.1016/j.ebiom.2019.03.016.
57. Clayton A, Mason MD. Exosomes in tumour immunity. *Curr Oncol.* 2009;16(3):46–49. doi:10.3747/co.v16i3.367.
58. Yang C, Robbins PD. The roles of tumor-derived exosomes in cancer pathogenesis. *Clin Dev Immunol.* 2011;(2011):842849. doi:10.1155/2011/842849.
59. Collino F, Deregis MC, Bruno S, Sterpone L, Aghemo G, Viltono L, Tetta C, Camussi G. Microvesicles derived from adult human bone marrow and tissue specific mesenchymal stem cells shuttle selected pattern of miRNAs. *PLoS One.* 2010;5(7):e11803. doi:10.1371/journal.pone.0011803.
60. Guduric-Fuchs J, O'Connor A, Camp B, O'Neill CL, Medina RJ, Simpson DA. Selective extracellular vesicle-mediated export of an overlapping set of microRNAs from multiple cell types. *BMC Genomics.* 2012;13(1):357. doi:10.1186/1471-2164-13-357.
61. Ohshima K, Inoue K, Fujiwara A, Hatakeyama K, Kanto K, Watanabe Y, Muramatsu K, Fukuda Y, Ogura S, Yamaguchi K, *et al.* Let-7 microRNA family is selectively secreted into the extracellular environment via exosomes in a metastatic gastric cancer cell line. *PLoS One.* 2010;5(10):e13247. doi:10.1371/journal.pone.0013247.
62. Chen X, Liang H, Zhang J, Zen K, Zhang CY. microRNAs are ligands of Toll-like receptors. *RNA.* 2013;19(6):737–739. doi:10.1261/rna.036319.112.
63. Fabbri M. TLRs as miRNA receptors. *Cancer Res.* 2012;72(24):6333–6337. doi:10.1158/0008-5472.CAN-12-3229.
64. Fabbri M, Paone A, Calore F, Galli R, Gaudio E, Santhanam R, Lovat F, Fadda P, Mao C, Nuovo GJ, *et al.* MicroRNAs bind to Toll-like receptors to induce prometastatic inflammatory response. *Proc Natl Acad Sci U S A.* 2012;109(31):E2110–2116. doi:10.1073/pnas.1209414109.
65. Lehmann SM, Kruger C, Park B, Derkow K, Rosenberger K, Baumgart J, Trimbuch T, Eom G, Hinz M, Kaul D, *et al.* An unconventional role for miRNA: let-7 activates Toll-like receptor 7 and causes neurodegeneration. *Nat Neurosci.* 2012;15(6):827–835. doi:10.1038/nn.3113.
66. Salvi V, Gianello V, Busatto S, Bergese P, Andreoli L, D'Oro U, Zingoni A, Tincani A, Sozzani S, Bosisio D. Exosome-delivered microRNAs promote IFN-alpha secretion by human plasmacytoid DCs via TLR7. *JCI Insight.* 2018;3(10):3. doi:10.1172/jci.insight.98204.
67. Gajewski TF, Schreiber H, Fu YX. Innate and adaptive immune cells in the tumor microenvironment. *Nat Immunol.* 2013;14(10):1014–1022. doi:10.1038/ni.2703.
68. Kalos M, June CH. Adoptive T cell transfer for cancer immunotherapy in the era of synthetic biology. *Immunity.* 2013;39(1):49–60. doi:10.1016/j.immuni.2013.07.002.
69. Kennedy BC, Maier LM, D'Amico R, Mandigo CE, Fontana EJ, Waziri A, Assanah MC, Canoll P, Anderson RC, Anderson DE, *et al.* Dynamics of central and peripheral immunomodulation in a murine glioma model. *BMC Immunol.* 2009;10(1):11. doi:10.1186/1471-2172-10-11.
70. Wraith DC, Nicholson LB. The adaptive immune system in diseases of the central nervous system. *J Clin Invest.* 2012;122(4):1172–1179. doi:10.1172/JCI58648.
71. Zirger JM, Puntel M, Bergeron J, Wibowo M, Moridzadeh R, Bondale N, Barcia C, Kroeger KM, Liu C, Castro MG, *et al.* Immune-mediated loss of transgene expression from virally transduced brain cells is irreversible, mediated by IFNgamma, perforin, and TNFalpha, and due to the elimination of transduced cells. *Mol Ther.* 2012;20(4):808–819. doi:10.1038/mt.2011.243.
72. Hasler D, Lehmann G, Murakawa Y, Klironomos F, Jakob L, Grasser FA, Rajewsky N, Landthaler M, Meister G. The Lupus Autoantigen La Prevents Mis-channeling of tRNA Fragments into the Human MicroRNA Pathway. *Mol Cell.* 2016;63(1):110–124. doi:10.1016/j.molcel.2016.05.026.
73. Babiarz JE, Ruby JG, Wang Y, Bartel DP, Blelloch R. Mouse ES cells express endogenous shRNAs, siRNAs, and other Microprocessor-independent, Dicer-dependent small RNAs. *Genes Dev.* 2008;22(20):2773–2785. doi:10.1101/gad.1705308.
74. Colak E, Leslie A, Zausmer K, Khatamzas E, Kubarenko AV, Pichulik T, Klimosch SN, Mayer A, Siggs O, Hector A, *et al.* RNA and imidazoquinolines are sensed by distinct TLR7/8 ectodomain sites resulting in functionally disparate signaling events. *J Immunol.* 2014;192(12):5963–5973. doi:10.4049/jimmunol.1303058.
75. Zhang Z, Ohto U, Shibata T, Krayukhina E, Taoka M, Yamauchi Y, Tanji H, Isobe T, Uchiyama S, Miyake K, *et al.* Structural Analysis Reveals that Toll-like Receptor 7 Is a Dual Receptor for Guanosine and Single-Stranded RNA. *Immunity.* 2016;45(4):737–748. doi:10.1016/j.immuni.2016.09.011.
76. Zhang Z, Ohto U, Shibata T, Taoka M, Yamauchi Y, Sato R, Shukla NM, David SA, Isobe T, Miyake K, *et al.* Structural Analyses of Toll-like Receptor 7 Reveal Detailed RNA Sequence Specificity and Recognition Mechanism of Agonistic Ligands. *Cell Rep.* 2018;25(12):3371–3381 e3375. doi:10.1016/j.celrep.2018.11.081.
77. Baker GJ, Castro MG, Lowenstein PR. Isolation and Flow Cytometric Analysis of Glioma-infiltrating Peripheral Blood Mononuclear Cells. *J Vis Exp.* 2015;105. doi:10.3791/53676.
78. Koschmann C, Calinescu AA, Nunez FJ, Mackay A, Fazal-Salom J, Thomas D, Mendez F, Kamran N, Dzaman M, Mulpuri L, *et al.* ATRX loss promotes tumor growth and impairs nonhomologous end joining DNA repair in glioma. *Sci Transl Med.* 2016;8(328):328ra328. doi:10.1126/scitranslmed.aac8228.
79. Nunez FJ, Mendez FM, Kadiyala P, Alghamri MS, Savelieff MG, Garcia-Fabiani MB, Haase S, Koschmann C, Calinescu AA, Kamran N, *et al.* IDH1-R132H acts as a tumor suppressor in glioma via epigenetic up-regulation of the DNA damage response. *Sci Transl Med.* 2019;11(479):eaaq1427. doi:10.1126/scitranslmed.aaq1427.
80. Oshlack A, Robinson MD, Young MD. From RNA-seq reads to differential expression results. *Genome Biol.* 2010;11(12):220. doi:10.1186/gb-2010-11-12-220.
81. Robinson MD, Oshlack A. A scaling normalization method for differential expression analysis of RNA-seq data. *Genome Biol.* 2010;11(3):R25. doi:10.1186/gb-2010-11-3-r25.